

Summer 2006

Theoretical Analysis of Transpiration Cooling of a Liquid Rocket Thrust Chamber Wall

Philip A. Davis
Embry-Riddle Aeronautical University - Daytona Beach

Follow this and additional works at: <https://commons.erau.edu/db-theses>



Part of the [Aeronautical Vehicles Commons](#)

Scholarly Commons Citation

Davis, Philip A., "Theoretical Analysis of Transpiration Cooling of a Liquid Rocket Thrust Chamber Wall" (2006). *Theses - Daytona Beach*. 38.

<https://commons.erau.edu/db-theses/38>

This thesis is brought to you for free and open access by Embry-Riddle Aeronautical University – Daytona Beach at ERAU Scholarly Commons. It has been accepted for inclusion in the Theses - Daytona Beach collection by an authorized administrator of ERAU Scholarly Commons. For more information, please contact commons@erau.edu.

THEORETICAL ANALYSIS OF TRANSPIRATION
COOLING OF A LIQUID ROCKET THRUST CHAMBER WALL

By

Philip A. Davis

A thesis Submitted to the
Physical Sciences Department
In Partial Fulfillment of the Requirements for the Degree of
Master of Science in Space Sciences

Embry-Riddle Aeronautical University
Daytona Beach, Florida
Summer 2006

UMI Number: EP32103

INFORMATION TO USERS

The quality of this reproduction is dependent upon the quality of the copy submitted. Broken or indistinct print, colored or poor quality illustrations and photographs, print bleed-through, substandard margins, and improper alignment can adversely affect reproduction.

In the unlikely event that the author did not send a complete manuscript and there are missing pages, these will be noted. Also, if unauthorized copyright material had to be removed, a note will indicate the deletion.

UMI[®]

UMI Microform EP32103
Copyright 2011 by ProQuest LLC
All rights reserved. This microform edition is protected against
unauthorized copying under Title 17, United States Code.

ProQuest LLC
789 East Eisenhower Parkway
P.O. Box 1346
Ann Arbor, MI 48106-1346

THEORETICAL ANALYSIS OF TRANSPIRATION
COOLING OF A LIQUID ROCKET THRUST CHAMBER WALL

by

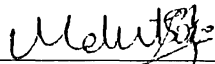
Philip A. Davis

This thesis was prepared under the direction of the candidate's thesis committee chair, Dr. Mehmet Sozen, Department of Physical Sciences, and has been approved by the members of his thesis committee. It was submitted to the Department of Physical Sciences and was accepted in partial fulfillment of the requirements for the

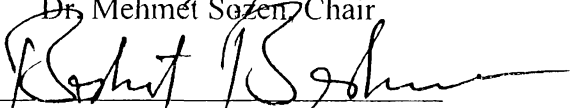
Degree of

Master of Science in Space Sciences

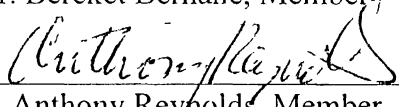
THESIS COMMITTEE:




Dr. Mehmet Sozen, Chair




Dr. Bereket Berhane, Member



Dr. Anthony Reynolds, Member



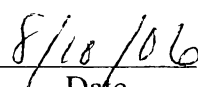
Dr. Peter Erdman, MSSPS Graduate Program Coordinator



Dr. John Olivero, Department Chair, Physical Sciences



Dr. Christina Frederick, Associate Provost



Date

Acknowledgements

This thesis is the culmination of two years of hard work that could not be completed without the help of the special people in my life. First and foremost, I would like to thank my parents, Greg and Dena, and my sister Laura for their unconditional love and support they have given me my entire life. Next I would like to thank my advisor, Dr. Mehmet Sozen for all of his effort and patience in helping me overcome some of the obstacles that occurred throughout the research process. The entire Physical Sciences Department at ERAU has been wonderful in nurturing my academic career and providing me with many opportunities to enhance my scholastic skills. Finally, I must thank my employers, Bill Maguire and Richie Allen at Peninsular Printing for providing me with the opportunity of employment while allowing me the freedom to pursue my academic career without interruption. I would also like to thank my co-workers especially Jeff Smith, Ralph Cennane, and Lisa Luangrathkhamkeo for the invaluable wisdom and life lessons they have taught me that have helped me become the person I am today.

Table of Contents

	Page
Acknowledgements.....	iii
Table of Contents.....	iv
List of Figures.....	vi
List of Tables.....	viii
List of Symbols.....	ix
Abstract.....	x
Chapter 1: Introduction.....	1
1.1 Thesis Statement.....	1
1.2 Background.....	1
1.3 Objectives and Scope.....	2
Chapter 2: Development of the Mathematical Model.....	6
2.1 Description of the Mathematical Model.....	6
2.2 Numerical Analysis of the Incompressible Flow Model.....	15
2.3 Numerical Analysis of the Compressible Flow Model.....	21
2.4 Developing the Code.....	24
Chapter 3: Model Comparison and General Results.....	29
3.1 Grid Size Sensitivity Analysis.....	29
3.2 General Results.....	33
3.3 Comparing the Results from the Two Models.....	36
Chapter 4: Parametric Studies.....	43
4.1 Basic Test Parameters.....	43

4.2 Effects of Varying the Porous Liner Thickness.....	45
4.3 Effects of Varying the Porosity of the Porous Liner.....	52
Chapter 5: Conclusions and Recommendations.....	58
5.1 Conclusions.....	58
5.2 Recommendations.....	60
References.....	62
Appendix A: Discretization of the Governing Equations and Boundary Condition by Finite Difference Approximations for the Incompressible Flow Model.....	63
Appendix B: Discretization of the Governing Equations and Boundary Condition by Finite Difference Approximations for the Compressible Flow Model.....	68
Appendix C: Incompressible Model FORTRAN Flowchart.....	69
Appendix D: Compressible Model FORTRAN Flowchart.....	70
Appendix E: Incompressible Flow Model FORTRAN Program.....	71
Appendix F: Compressible Flow Model FORTRAN Program.....	83

List of Figures

Figure	Page
1.1 Transpiration Cooling Model Developed at AFRL.....	3
2.1 Schematic of the Two Layered Simplified Geometry.....	6
2.2 Schematic of the Interface Boundary Conditions.....	14
2.3 Schematic of the Nodes used to describe the System.....	15
3.1 Temperature Distribution Results Using Five Different Numbers of Nodes.....	30
3.2 Velocity Distributions Results Using Five Different Numbers of Nodes	31
3.3 Pressure Distributions Results Using Five Different Numbers of Nodes	32
3.4 The Effects of Different Inlet Mass Flow Rates on the Temperature Distribution Across the Wall.....	34
3.5 The Effects of Different Inlet Mass Flow Rates on the Pressure Distribution Across the Wall.....	35
3.6 The Effects of Different Inlet Mass Flow Rates on the Velocity Distribution Across the Wall.....	36
3.7 Pressure Comparison between the Two Models.....	37
3.8 Density Comparison between the Two Models.....	38
3.9 Velocity Comparison between the Two Models.....	39
3.10 Comparison of the Mass Flow Rate for the Two Models.....	40
3.11 Temperature Comparison for the Two Models.....	41
4.1 Typical Pressure Distribution for Varying Liner Thickness.....	46
4.2 Pressure Drop Comparison for the Varying Liner Thickness.....	48
4.3 Temperature Distributions for the Four cases with a .048 kg/s Inlet Mass Flow Rate and a 30.000 W/m ² Heat Flux.....	49

4.4 Temperature Distributions for the Four cases with a .38 kg/s Inlet Mass Flow Rate and a 30,000 W/m ² Heat Flux.....	49
4.5 Temperature Distributions for the Four cases with a .76 kg/s Inlet Mass Flow Rate and a 30,000 W/m ² Heat Flux.....	50
4.6 Maximum Heat Flux for the Different Liner Thickness Cases for Varying Mass Flow Rates.....	51
4.7 Pressure Distribution for the Varying Porosity Cases.....	53
4.8 Pressure Drop Comparison for the Varying Liner Porosity Cases.....	54
4.9 Typical Temperature Distribution for the Varying Liner Porosity Cases.....	55
4.10 Maximum Heat Flux for the Different Liner Porosity Cases for Varying Mass Flow Rates.....	56

List of Tables

Table	Page
3.1 Relative Temperature Difference at the Hot Gas Boundary for Varying Grid Spaces.....	30
3.2 Relative Velocity Difference at the Hot Gas Boundary for Varying Grid Spaces.....	31
3.3 Relative Pressure Difference at the Hot Gas Boundary for Varying Grid Spaces.....	32
4.1 Hydrogen Properties.....	44
4.2 Properties of the Porous Foam and Liner for the Varying Thickness Analysis.....	45
4.3 Maximum Mass Flow Rate for Varying Liner Thickness.....	47
4.4 Maximum Mass Flow Rates for Varying Liner Porosities.....	54
4.5 Maximum Allowable Heat Flux for the Various Liner Porosity Cases.....	57

List of Symbols

Symbol		Units
u	Darcy Velocity	m/s
ρ	Density	kg/m ³
R	Gas Constant	J/(kg · K)
q''	Hot Gas Boundary Heat Flux	W/m ²
\dot{m}	Mass Flow Rate	kg/s
α	Permeability Coefficient	
β	Permeability Coefficient	
D_p	Pore Diameter of Spheres in Packed Bed	m
ε	Porosity	
P	Pressure	Pa
c_p	Specific Heat	J/(kg · K)
T	Temperature	K
k	Thermal Conductivity	W/(m · K)
A_{total}	Total Cross Section Area	m ²
μ	Viscosity	Pa · s

Subscripts

f	Coolant Fluid
A	General Porous Matrix. Either Porous Liner or Porous Foam
s	Porous Solid
1	Porous Foam
2	Porous Liner

Abstract

Author: Philip A. Davis
Title: Theoretical Analysis of Transpiration Cooling of a Liquid Rocket Thrust Chamber Wall
Institution: Embry-Riddle Aeronautical University
Degree: Master of Science in Space Sciences
Year: 2006

Transpiration cooling is a process that could reduce the overall weight of the cooling system of an actively cooled thrust chamber wall of a liquid rocket engine by up to 50% when compared to other active cooling techniques, increasing the thrust to weight ratio of the rocket engine. In this thesis, mathematical models and computer codes were developed for simulating the flow of a coolant and the transport phenomena in a transpiration cooled thrust chamber wall of a liquid rocket engine by treating the coolant in two ways: as an incompressible fluid and as a compressible fluid in local thermal equilibrium with the porous structures that make up the thrust chamber wall. The programs were run with similar conditions and the results show that the incompressible flow model is a useful tool for accurately determining the temperature distribution inside the thrust chamber wall. The incompressible flow model was also used to perform parametric studies involving varying the thickness and porosity of the porous liner section of the wall. The results of these parametric studies show that varying the thickness and/or porosity of the porous liner can be utilized as a means for controlling the flow of the coolant inside the wall as well as its general function as a structural support for the thrust chamber wall.

Chapter 1 Introduction

1.1 Thesis Statement

The purpose of this thesis is to develop a program to theoretically analyze the behavior of a coolant fluid as well as the temperature distribution inside the thrust chamber wall of a transpiration cooled liquid rocket engine.

1.2 Background

When designing the thrust chamber of a rocket engine, it is important to implement a proper cooling technique for the thrust chamber wall. Cooling the thrust chamber wall prevents the wall from becoming too hot, keeping the wall within the load and stress limits its materials allow. With increased temperature, the chamber wall loses strength and faces the possibility of failing or melting. The cooling process also helps to reduce the oxidation of the wall material and the rate at which the wall's material degrades.

The different cooling techniques that are commonly found in liquid rocket engines fall into two main categories, the steady state method and transient heat transfer method. (Sutton 2001) The main cooling techniques that fall in the category of the steady state method are regenerative cooling and radiation cooling. Regenerative cooling involves building a cooling jacket around the thrust chamber wall. Liquid coolant is then fed through this cooling jacket before it is fed into the injector. Regenerative cooling is currently used in the Space Shuttle Main Engines (SSME) and is used in applications with high chamber pressures and high heat transfer rates. Radiation cooling involves the use of high temperature materials for the thrust chamber wall. When the wall reaches

thermal equilibrium it radiates the heat from the thrust propellants to the surrounding area. This technique is effective for engines with low chamber pressures and moderate heat transfer rates. As its name suggests, the transient heat transfer method does not involve the chamber wall reaching a steady state temperature. The chamber wall in this case is used as a heat sink. The temperature of the wall continues to rise throughout the duration of operation and the heat is absorbed in an inner liner of ablative material. Since thermal equilibrium at the wall is not reached, there is a finite amount of time that the engine can operate before the wall reaches its material limits.

Transpiration cooling, or film cooling, is a technique that can fall into either category. Transpiration cooling involves the use of a liner similar to that in the transient heat transfer method as well as the injection of a coolant as in the case of regenerative cooling. A porous material or a combination of porous materials is imbedded inside of the thrust chamber wall. A coolant fluid, typically the propellant, is then pushed through the porous material until it ultimately reaches the thrust chamber wall. The thermal properties, most notably the effective thermal conductivity, of the coolant and porous matrix provide an efficient cooling mechanism for the thrust chamber wall.

1.3 Objectives and Scope of the Thesis

The idea for this research is based on the work done at the German Aerospace Center (DLR) and the work done by the Air Force Research Lab (AFRL) at Wright Air Force Base. The concepts being researched at AFRL are a part of the Integrated High-Payoff Rocket Propulsion Technology Program (IHRPT) and involve the use of transpiration

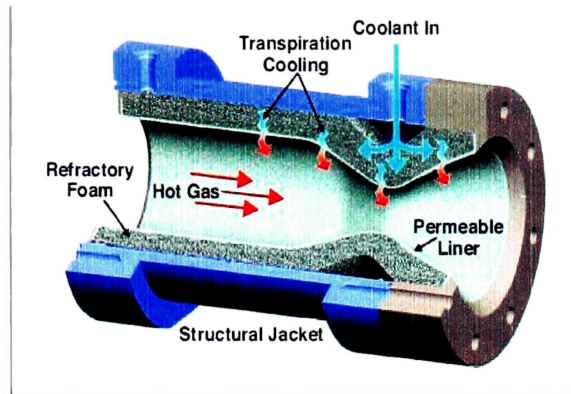


Figure 1.1: Transpiration Cooling Model Developed at AFRL (Steel 2004)

cooling as a way to improve current, actively cooled thrust chambers. (Steel 2004) The AFRL concept involves the use of a two porous matrix system, a porous inner liner and an intermediate lightweight porous foam coolant plenum as shown in Figure 1.1. The researchers believe that the use of this transpiration cooled system can reduce the weight of current cooling systems up to 50% while also reducing the system cost, part count, and coolant volume.

Currently, AFRL is partnering with a private company called Ultramet to develop a transpiration system using metallic porous matrices and ceramic porous matrices. At the German Aerospace Center (DLR) research has been performed on the benefits of using ceramic liners in transpiration cooled cryogenic liquid rocket engine. The researchers at DLR claim that improvement in ceramic-matrix-composite (CMC) technologies would allow for a larger growth potential than current active cooling technology. (Greuel 2004) The researchers at DLR also make the same claims as the researchers at AFRL in that transpiration cooling has the potential to decrease the weight of the thrust chamber, improving the thrust to weight ratio of a liquid rocket that requires active cooling.

This thesis is a theoretical extension of the work of the researchers at DLR and AFRL. A geometrically simplified transpiration cooled thrust chamber wall is modeled using both a two-layered system consisting of porous foam coupled with a porous interior liner as shown in Figure 1, and as a system containing only one porous matrix. The addition of a porous liner, thus making the model a two-layered system, can be used to control the flow of the coolant in addition to providing structural integrity to the wall. The porous liner can be made up of the same material with different properties as the porous foam, or be comprised of a different material. One of the objectives of this thesis is to determine if there is any general behavior pattern when the thickness and porosity of the porous liner section is varied. The material used for both porous matrices will be Si-C, a ceramic being developed by Ultramet for the research to be done at AFRL. The thermal and physical properties that are used in this study have been obtained from the Ultramet website, www.ultramet.com, as well as Ultramet publications (Brockmeyer 1998). The fluid being used as the coolant in the system is supercritical hydrogen. The thermal properties for the hydrogen have been obtained from the National Institute of Standards and Technology (NIST) and can be found at www.nist.gov. The values for all of the properties of supercritical hydrogen were not available for the full range of temperatures that were expected. In these cases, an average value for each of the specific properties was used in the model.

The flow of supercritical hydrogen through the porous thrust chamber wall along with the transport phenomena were modeled in two ways. The first model, the compressible flow

model accounts for the compressibility effects of the fluid as it flows radially from the coolant reservoir to the thrust chamber. The second model, the incompressible fluid flow model, ignores the compressibility effects of the fluid and assumes that the density of the fluid remains constant at all points inside the thrust chamber wall. The equations that form the mathematical model were solved numerically using finite difference methods. A sensitivity analysis was performed to determine how the chosen grid size affects the results of the simulation. To determine the effectiveness of the results using the incompressible model, a test case was set to compare the results for the two models. In the test case, a single porous matrix was used and the properties of the Si-C foam were used for the study. Two major parametric studies were carried out. The first case involves varying the thickness of the porous liner section and comparing those results to a single porous matrix system. The thickness of the porous liner section varies from 10% of the total thrust chamber wall thickness to 30% of the total thickness. The second case explores the behavior of the fluid when the porosity of the porous liner section is varied. By changing the porosity of the liner, the effective thermal conductivity of the coolant and porous matrix system and the flow of the fluid in the liner section were varied. The porosities studied range from 20% to 30% for the porous liner section compared to the porous foam section, which has a porosity of 50%. Due to CPU run-time constraints, the parametric studies were performed using the incompressible flow model.

Chapter 2: Development of the Mathematical Model

2.1 Description of the Mathematical Model

In this chapter the equations that define the behaviors of the coolant fluid and the porous wall of the thrust chamber used for transpiration cooling are established. The model involves the usual conservation principles used in the analysis of transport phenomena as they apply in porous media. These are the conservation of mass, momentum, and energy.

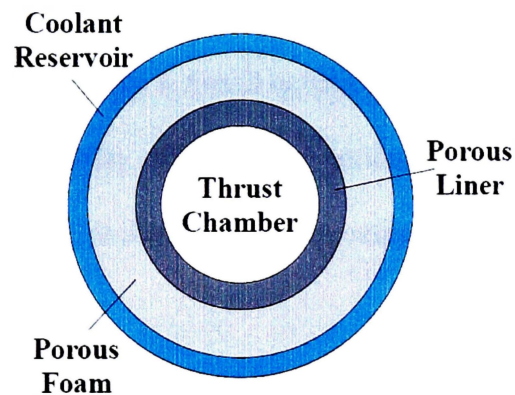


Figure 2.1: Schematic of the Two Layered Simplified Geometric Model

The behavior of the coolant fluid and the porous media inside the thrust chamber wall are determined from the geometrical parameters of the porous matrices, the operational boundary conditions, and the thermophysical properties of the coolant and the porous matrices. The mathematical model is a one-dimensional model for a simplified cylindrical geometry used to replace the actual geometry as shown in Figure 1.1. Figure 2.1 shows the schematic diagram for the thrust chamber wall using the simplified geometry. For the simulations that were performed in this thesis, the thrust chamber was assumed to have a radius of 15.0 cm and the thrust chamber wall was assumed to have a thickness of 6.0 cm. The length of the thrust chamber was specified to be 1.0 m. The

thrust chamber wall as shown in this figure consists of two layered porous structures, a porous liner and a porous foam. The porous liner and porous foam are both made of the same material but have different physical properties due to different porosities. The inner wall of the thrust chamber represents the hot gas boundary. The interior interface boundary is the point where the porous liner intersects the porous foam. At the point where the porous foam intersects with the coolant reservoir is the cold gas boundary. In each of the two models, compressible and incompressible fluid flow, the conservation of mass, momentum, and energy equations are required to model the coolant behavior. In the case of compressible fluid flow, a fourth equation, the equation of state, is introduced to account for the compressibility effects. The coolant is supercritical hydrogen and is modeled as an ideal gas. In what follows, these equations are presented in detail.

The Continuity Equation

The conservation of mass equation for a one-dimensional radial flow through a porous medium is

$$\varepsilon_A \frac{\partial \rho_f}{\partial t} + \frac{1}{r} \frac{\partial}{\partial r} (r \rho_f u_f) = 0 \quad (1)$$

The quantity ε_A is the porosity of the porous matrix, which is assumed to be an isotropic medium, and u_f refers to the Darcy velocity of the coolant fluid. The subscript, A, is used to generalize the equations used to describe the flow through the porous matrices. In the cases where both a porous liner and a porous foam are used, subscript 1 will be used in reference to the porous foam; whereas subscript 2 will be used in reference to the porous liner. The porosity of the material, also referred to as the void fraction, is the

proportion of the non-solid volume to the total volume of a porous medium. The Darcy velocity is a volume-averaged velocity as opposed to the mean pore velocity. The relation between the Darcy velocity and the mean pore velocity, v_f , is $u_f = \varepsilon_A v_f$. Even though the steady state solution is desired, the unsteady state governing equation is used in the compressible flow case because this provides a convenient solution method through the use of an explicit scheme using finite difference methods. Choosing small time steps ensures the stability of the solution. The continuity equation is used to solve for the fluid density in the compressible flow model. By definition, the density of a fluid in an incompressible flow case is constant. Therefore, in the incompressible flow case, the transient term is identically zero and the continuity equation becomes

$$\frac{\partial}{\partial r}(r u_f) = 0 \quad (2)$$

In the incompressible flow model, the continuity equation is used to solve for the Darcy velocity of the fluid.

The Conservation of Momentum Equation

The conservation of momentum equation for a one-dimensional radial flow through a porous matrix in cylindrical coordinates is

$$\frac{1}{\varepsilon_A} \frac{\partial}{\partial t}(\rho_f u_f) = -\frac{\partial P_f}{\partial r} - \left(\frac{\mu_f}{\alpha_A} + \frac{\rho_f}{\beta_A} |u_f| \right) u_f \quad (3)$$

This momentum equation is an adaptation of the equation,

$$\frac{\partial P}{\partial r} = -\frac{\mu}{\alpha} u_f \quad (4)$$

originally developed by Henry Darcy in 1856 (Greuel 2004) known as Darcy flow. The coefficients α and β are permeability coefficients. These coefficients depend on the properties of the porous matrix. Assuming that the porous matrix is comprised of a packed bed of spheres, the permeability coefficients can be approximated as (Sozen 1994)

$$\alpha_A = \frac{D_{p_i}^2 \varepsilon_A^3}{150(1 - \varepsilon_A)^2}, \quad (5)$$

$$\beta_A = \frac{D_{p_i} \varepsilon_A^3}{1.75(1 - \varepsilon_A)}, \quad (6)$$

where the quantity D_p refers to the mean pore diameter of the porous matrices. The momentum equation is used to solve for the Darcy velocity in the compressible flow model. In the incompressible flow case, the transient term is not used to determine the steady state solution and the conservation of momentum equation used in this case reduces to

$$\frac{\partial P}{\partial r} = - \left(\frac{\mu_f}{\alpha_A} + \frac{\rho_f}{\beta_A} |u_f| \right) u_f \quad (7)$$

The first term in the parenthesis on the right hand side of this equation represents the viscous drag with the term μ_f representing the viscosity of the coolant while the second term in parenthesis represents the form drag. In the incompressible flow model, the fluid pressure is determined from the momentum equation.

The Conservation of Energy Equation

Unlike the conservation of momentum and mass equations, the transient energy equation is used for both the incompressible and compressible fluid flow models. For the energy equation, an assumption of local thermal equilibrium between the solid porous matrices and the coolant fluid is used. This assumption results in a simple, one-dimensional energy equation written as

$$\left(\rho c_p\right)_A \frac{\partial T}{\partial t} + \varepsilon_A \rho_f u_f c_{p_f} \frac{\partial T}{\partial r} = \frac{1}{r} \frac{\partial}{\partial r} \left(k_{A,r} \frac{\partial T}{\partial r} \right) \quad (8)$$

The first term on the left hand side of the equation is the transient term where $\left(\rho c_p\right)_A$ is approximated as

$$\left(\rho c_p\right)_A = (1 - \varepsilon_A) \rho_s c_{p_s} + \varepsilon_A \rho_f c_{p_f} \quad (9)$$

The second term on the left hand side of equation (8) is the convective term which represents the transport of thermal energy by the bulk motion of the fluid, advection. The term on the right hand side of the equation is the conduction term, representing the transport of thermal energy by diffusion. The term $k_{A,r}$ is the effective thermal conductivity of the solid and fluid phases in local thermal equilibrium and the term c_p represents the specific heat capacity. There are several empirical models for the effective thermal conductivity of a fluid saturated porous medium. The approximation for the effective thermal conductivity of the system used in this thesis is the same approximation used by Landis (Landis 1995) based on the model derived by Chi (Chi, 1976) in his book on heat pipe theory. Accordingly, the effective thermal conductivity is approximated as

$$k_{A,r} = \frac{k_f \left[(2k_f + k_{s,r}) - 2(1 - \varepsilon_A)(k_f - k_{s,r}) \right]}{2k_f + k_{s,r} + (1 - \varepsilon_A)(k_f - k_{s,r})}, \quad (10)$$

where k_f is the thermal conductivity of the supercritical hydrogen, and k_s is the thermal conductivity of the porous matrix. The energy equation is used to solve for the temperature distribution in each of the two models.

The State Equation

Although it is necessary to only solve equations (2), (7), and (8) to determine the coolant behavior and the temperature distribution across the thickness of the thrust chamber wall using the incompressible flow model, a fourth equation must be introduced for closure of the mathematical model for the compressible flow case. The final governing equation is the equation of state. Assuming that the coolant behaves as a supercritical fluid, the ideal gas law is used as the final governing equation and is written as

$$P_f = \rho_f R_f T_f \quad (11)$$

The term R_f is the coolant gas constant. The compressibility factor of a gas is a function of its reduced temperature and reduced pressure. The range of temperatures used in the current work is 290-1500 K, while the range of pressure used is 1.31-1.35 MPa. These yield reduced temperatures in the range of 8.71-45.0 and reduced pressures in the range of 1.008-1.038. These reduced temperatures and pressures result in compressibility factor ranging between 1.00191-1.00841. Therefore the assumption of ideal gas behavior for the coolant is very well justified.

Boundary Conditions

The thrust chamber wall used in the incompressible model consists of two, layered porous matrices. This results in three sets of boundary conditions that are necessary to

define the model. First are the cold gas boundary conditions, which represent the coolant reservoir conditions. At the inlet several conditions must be met to ensure that the model remains valid. The first condition is that the coolant is assumed to be a supercritical fluid; therefore it must have properties of a supercritical fluid. The coolant used in this analysis is supercritical hydrogen, which must maintain a pressure of at least 1.30 MPa. A constant boundary pressure of 1.35 MPa, as well as a constant boundary temperature of 290 K is set for both models. The equation of state is used to determine the density at the cold gas boundary in the compressible flow model and is written as

$$\rho_n = \frac{P_n}{R_f T_n} \quad (12)$$

Different methods are used for determining the velocity at the inlet for the two different models. For the incompressible model, the velocity will be determined from a predefined fluid mass flow rate. The Darcy velocity at the inlet boundary in the incompressible flow model was obtained from

$$u_f = \frac{\dot{m}_f}{\rho_f A_{total}}, \quad (13)$$

where \dot{m}_f is the inlet mass flow rate of the coolant coming from the coolant reservoir, ρ_f is the density of supercritical hydrogen, and A_{total} is the area of the thrust chamber wall at the cold gas boundary. The inlet mass flow rate plays an integral part in the coolant behavior and temperature distribution inside the thrust chamber wall. The structural and thermal properties of the porous matrices as well as the thermal properties of the coolant fluid will determine how much the mass flow rate can be “throttled down” while still providing an effective cooling mechanism. For the compressible flow case, the Darcy velocity at the cold gas boundary is determined from the momentum equation using finite

difference approximations. By varying the cold gas boundary pressure, there will be a variance on how much the pressure gradient “pushes” the coolant through the porous matrix.

At the inner wall, the only boundary condition in the incompressible model is a constant heat flux that represents the heat input per unit area from the combustion products to the chamber wall and coolant system. For a given heat flux, the boundary condition for the energy equation takes the following form

$$q'' = k_A \frac{\partial T}{\partial r}, \quad (14)$$

where the quantity q'' is the constant hot gas boundary heat flux. The hot gas boundary heat flux, along with the inlet coolant mass flow rate, is one of the main parameters of study in this thesis. The heat flux varies with different engines and the magnitude of the heat flux, as well as the material properties, determine the inlet coolant mass flow rate necessary to ensure that the porous wall remains within its thermal and structural limits. Forward differencing was used to solve for the density and pressure of the coolant from the continuity and momentum equations respectively in the incompressible model at the hot gas boundary. For the compressible flow model, the density of the fluid was determined from the continuity equation, the velocity was obtained from the momentum equation, and the pressure at the hot gas boundary was specified to be 1.31 MPa.

For the cases where a two-layered porous matrix system was used for modeling the thrust chamber wall, a third set of boundary conditions is required. These include the continuity of pressure, temperature, and radial flow (Ngo 1998). The temperature of the system at

the interior boundary can be determined through an energy balance at the interface between the two porous layers and can be written as

$$k_1 \left. \frac{\partial T_1}{\partial r} \right|_{Interface} = k_2 \left. \frac{\partial T_2}{\partial r} \right|_{Interface} \quad (15)$$

In this equation, k_1 and k_2 represent the effective thermal conductivity in the porous foam and porous liner sections respectively. The temperature gradient $\partial T_1 / \partial r$ refers to the rate of change in the temperature with respect to the porous foam section of the chamber wall and is discretized with a forward difference method. The temperature gradient $\partial T_2 / \partial r$ refers to the rate of change in temperature with respect to the porous liner section and is discretized using a backward difference method. The coolant density and velocity can be determined from the following conditions,

$$P_1 = P_2 \quad (16)$$

$$u_1 = u_2 \quad (17)$$

where P_1 and u_1 are the fluid pressure and Darcy velocity as calculated using the properties of the porous foam section, and P_2 and u_2 are the fluid pressure and Darcy

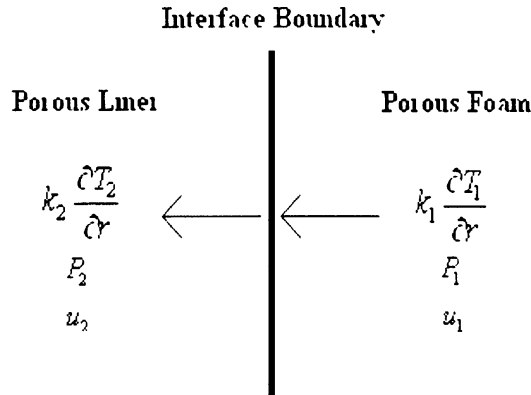


Figure 2.2: Schematic of the Interface Boundary Conditions

velocity as calculated using the properties of the porous liner section as shown in Figure 2.2. In the incompressible flow model, the velocity at each interior node is determined from the continuity equation while the pressure is determined from the momentum equation. At the interface boundary, the velocity and pressure are determined by discretizing these equations using a forward difference method to solve for P_1 and u_1 using the properties of the porous foam and a backward difference method to solve for P_2 and u_2 using the properties of the porous liner. The corresponding finite difference expressions are found in Appendix A. The discretized equations are then set equal to each other and solved for the values of the variables at the interface boundary. The energy balance is used to ensure that the same amount of energy that goes into the interface comes out of the interface. Since there is continuity of density at the interface, the boundary condition $u_1 = u_2$ ensures that the mass flow is constant across the interface boundary.

Initial Conditions

For the compressible flow model the only initial condition used was a uniform temperature of 290 K throughout the entire thickness of the thrust chamber wall. For the incompressible flow model, in addition to a uniform temperature of 290 K throughout the entire thickness of the wall, a uniform initial pressure of 1.31 MPa and a uniform Darcy velocity of 0.0 m/s were used throughout the entire thickness of the wall. The initial condition for the density distribution was determined from the ideal gas law and the pre-defined temperature and pressure profiles.

2.2 Numerical Analysis of the Incompressible Flow Model

In each of the mathematical models, there is coupling among the variables to be solved. A series of finite difference methods were used to solve these equations numerically. The development of the discretized equations for the incompressible model equations that are described hereafter are provided in Appendix A. Figure 2.3 is a schematic showing

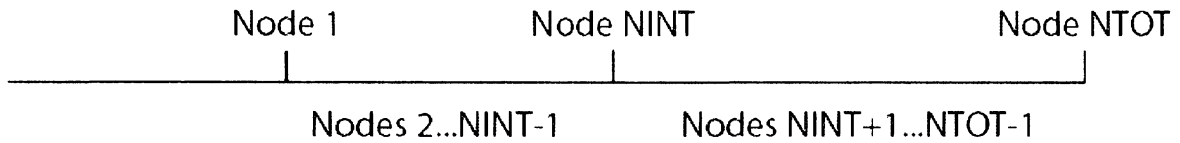


Figure 2.3: Schematic of the Nodes used to describe the System

how the nodes are labeled starting with node 1, which represents the hot gas boundary and ending with node NTOT, which represents the cold gas boundary. Since the density of the coolant is constant in the incompressible fluid flow model, the state equation is not used to determine the density of the coolant inside the thrust chamber wall. Upwind differencing is used to approximate the convective term in the continuity equation for the Darcy velocity of the fluid. Upwind differencing is the method that is commonly used to approximate the convective terms in order to make the numerical scheme stable. Because the flow of the coolant is in the negative r-direction, forward differencing corresponds to upwind differencing. For this analysis, all spatial derivatives are approximated with second order accurate schemes. The second order accurate forward differencing scheme used is

$$\frac{\partial X_n^m}{\partial r} = \frac{-3X_n^m + 4X_{n+1}^m - X_{n+2}^m}{2\Delta r}, \quad (18)$$

where X denotes any property that could be solved for and the superscript m refers to the time step. All cold gas boundary conditions are defined and constant. So there is no

need to apply any finite differencing techniques here. The second order accurate scheme must be modified in two locations in order to accommodate the model. The first such instance occurs at the node NTOT-1, which corresponds to the first node in from the cold gas boundary. Since this node has only one other available node upwind of it, there would be a conflict in trying to use the differencing scheme previously mentioned. The approach taken to solve for the velocity and pressure at this node was to perform a second order accurate backward differencing approximation on the node NTOT corresponding to the cold gas boundary. The second order accurate backward differencing scheme yields

$$\frac{\partial X_n^m}{\partial r} = \frac{3X_n^m - 4X_{n-1}^m + X_{n-2}^m}{2\Delta r} \quad (19)$$

In order to solve for the variables at node NTOT-1 and still keep a second order accurate scheme, the momentum and continuity equations are solved by taking the backward difference approximation for the spatial derivatives at the cold gas boundary and solving the equations for X_{n-1}^m . When this task is performed the approximation for the velocity and pressure at the nodes NTOT-1 became

$$u_{NTOT-1} = \frac{3r_{NTOT}u_{NTOT} + r_{NTOT-2}u_{NTOT-2}}{4r_{NTOT}} \quad (20)$$

$$P_{NTOT-1} = \frac{(3P_{NTOT} + P_{NTOT-2})}{4} + \left(\frac{\Delta r \mu_f}{2\alpha} \right) u_{NTOT} + \left(\frac{\Delta r \rho_f}{2\beta} \right) |u_{NTOT}| u_{NTOT} \quad (21)$$

The expressions in equations (20) and (22) are obtained from the continuity equation for the Darcy velocity, and equations (21) and (23) are obtained from the momentum equation for the fluid pressure. For the rest of the interior nodes in the porous foam, forward difference approximations are used for all spatial derivative terms in the

continuity and momentum equations. The finite difference approximations for the velocity and pressure at the interior nodes of the porous foam are

$$u_n = \frac{4r_{n+1}u_{n+1} - r_{n+2}u_{n+2}}{3r_n} \quad (22)$$

$$P_n = \left(\frac{4P_{n+1} - P_{n+2}}{3} \right) + \frac{2\Delta r \mu}{3\alpha_1} u_n + \frac{2\Delta r \rho}{3\beta_1} |u_n| u_n \quad (23)$$

Implementing the boundary conditions to solve for the pressure and Darcy velocity at the interface boundary node requires the use of forward and backward differencing. The boundary conditions state that both $u_1 = u_2$, and $P_1 = P_2$, as described in the previous section, must be satisfied at the interface boundary. To satisfy these conditions, the forward differencing scheme is applied at node NINT to approximate the value of u_1 and P_1 using the information from the porous foam domain. The backward difference approximation is used to solve for the values of u_2 and P_2 using the information from the porous liner domain. Then the approximations for u_1 and u_2 are set equal to each other yielding the expression

$$-3r_n u_n + 4r_{n+1} u_{n+1} - r_{n+2} u_{n+2} = 3r_n u_n - 4r_{n-1} u_{n-1} + r_{n-2} u_{n-2}, \quad (24)$$

which gives the approximation for the Darcy velocity at the interior boundary as,

$$u_n = \frac{1}{6r_n} (-r_{n-2} u_{n-2} + 4r_{n-1} u_{n-1} + 4r_{n+1} u_{n+1} - r_{n+2} u_{n+2}) \quad (25)$$

The same process is used in the momentum equation yielding the expression for the fluid pressure at the interface boundary as

$$P_n = \frac{1}{6} (-P_{n-2} + 4P_{n-1} + 4P_{n+1} - P_{n+2}) + \left(\frac{\Delta r \mu}{3(\alpha_1 - \alpha_2)} \right) u_n + \left(\frac{\Delta r \rho}{3(\beta_1 - \beta_2)} \right) |u_n| u_n \quad (26)$$

The second point where the modified finite difference approximations need to be used occurs at the node NINT-1. If the standard forward difference approximation were to be used here, then the solution would call for the approximations of the velocity and pressure in the porous liner, at the interface boundary, as well as the porous foam. In order to eliminate the need for the values at the porous foam, the same method used to solve for the velocity and pressure at node NTOT-1 will be applied to the node NINT-1.

The velocity and pressure approximations at node NINT-1 are

$$u_{NINT-1} = \frac{4r_{NINT}u_{NINT} - r_{NINT-2}u_{NINT-2}}{3r_{NINT}} \quad (27)$$

$$P_{NINT-1} = \frac{1}{4}(3P_{NINT} + P_{NINT-2}) + \left(\frac{\Delta r \mu_l}{2\alpha_2}\right)u_{NINT} + \left(\frac{\Delta r \rho_l}{2\beta_2}\right)|u_{NINT}|u_{NINT} \quad (28)$$

The variables for the remaining interior nodes in the porous liner, as well as the variables at the hot gas boundaries are obtained using the same forward difference approximations used in the porous foam section and are very similar to the approximations used for the interior nodes of the porous foam section. The only difference is that the thermal and physical properties of the foam have been replaced by the properties of the liner. The finite difference approximations for the Darcy velocity and pressure are

$$u_n = \frac{4r_{n+1}u_{n+1} - r_{n+2}u_{n+2}}{3r_n} \quad (29)$$

$$P_n = \left(\frac{4P_{n+1} - P_{n+2}}{3}\right) + \frac{2\Delta r \mu}{3\alpha_2}u_n + \frac{2\Delta r \rho}{3\beta_2}|u_n|u_n \quad (30)$$

A different approach is used to solve the energy equation to obtain the porous matrix temperature distribution. The first and most apparent difference is the use of the transient

energy equation to solve for the coolant and porous matrix temperature. This approach provides a convenient solution procedure for the energy equation. This method has a drawback in that in order to maintain stability in the solution, there is a limitation on the time step that can be used in the temporal derivative term. The temporal derivatives are approximated using first order forward differencing and appear as

$$\frac{\partial T_n^m}{\partial t} = \frac{T_n^{m+1} - T_n^m}{\Delta t} \quad (31)$$

Here the superscript m represents the value at the current known time step and the superscript $m+1$ represents the value at the time step to be solved. Second order centered differencing approximations are used to approximate the spatial derivatives. The first spatial derivative is approximated using the formula

$$\frac{\partial X_n^m}{\partial r} = \frac{X_{n+1}^m - X_{n-1}^m}{2\Delta r} \quad (32)$$

The approximation for the second spatial derivative required a more complex technique. The approximation uses not only the neighbors of any interior node, n , but also the midpoints between the nodes. The term

$$\frac{1}{r} \frac{\partial}{\partial r} \left(k_A r \frac{\partial T}{\partial r} \right)$$

is approximated as

$$\frac{1}{r} \frac{\partial}{\partial r} \left(r k_A \frac{\partial T}{\partial r} \right) = \frac{1}{r_n} \left[\frac{r_{n+1/2} k_A T_{n+1} - (r_{n+1/2} + r_{n-1/2}) k_A T_n + r_{n-1/2} k_A T_{n-1}}{(\Delta r)^2} \right] \quad (33)$$

When all of the finite difference approximations are put together, the expression for the system temperature at a typical interior node yields

$$T_n^{m+1} = \left[\frac{\Delta t r_{n-1/2} k_A}{(\rho c_p)_A r_n \Delta r^2} + \frac{\Delta t \varepsilon_A \rho_n^m u_n^m c_{p_f}}{2(\rho c_p)_A \Delta r} \right] T_{n-1}^m + \left[1 - \frac{\Delta t (r_{n+1/2} + r_{n-1/2}) k_A}{(\rho c_p)_A r_n \Delta r^2} \right] T_n^m + \left[\frac{\Delta t r_{n+1/2} k_A}{(\rho c_p)_A r_n \Delta r^2} - \frac{\Delta t \varepsilon_A \rho_n^m u_n^m c_{p_f}}{2(\rho c_p)_A \Delta r} \right] T_{n+1}^m \quad (34)$$

The method used to apply the energy balance at the interior boundary is similar to that used for the continuity and momentum equation. At the interface boundary, the condition that is implemented is an energy balance across the boundary, which is given as

$$k_1 \left. \frac{\partial T_1}{\partial r} \right|_{Interface} = k_2 \left. \frac{\partial T_2}{\partial r} \right|_{Interface}$$

Second order accurate forward and backward difference approximations are used to implement the energy balance at the interior interface yielding

$$T_n^{m+1} = \frac{1}{3(k_1 + k_2)} \left[-k_2 T_{n-2}^{m+1} + 4k_2 T_{n-1}^{m+1} + 4 \cdot k_1 T_{n+1}^{m+1} - k_1 T_{n+2}^{m+1} \right] \quad (35)$$

Note that all temperature values used are those that are evaluated at the $m+1$ time step. In order to correctly approximate the temperature at the interior boundary node, the temperatures of the interior nodes in both the liner and foam sections must be calculated before the temperature of the porous matrix at the interface boundary can be approximated.

Second order accurate forward difference approximation is used to implement the hot gas boundary condition

$$q'' = k_2 \left. \frac{\partial T}{\partial r} \right|_{HGB} \quad , \quad (36)$$

where the constant hot gas boundary heat flux is specified, giving the solution for the temperature of the system at the hot gas boundary as

$$T_1^{m+1} = -\frac{1}{3}T_3^{m+1} + \frac{4}{3}T_2^{m+1} - \left(\frac{2 \cdot \Delta r}{3 \cdot k_2}\right)q'' \quad (37)$$

These equations, coupled with the already defined variables at the cold gas boundary, allow for the approximation of each of the three variables at all nodes throughout the rocket engine wall. The finite difference approximations presented for the velocity and pressure are only valid for the incompressible fluid model while the finite difference approximations presented for the temperature are also valid in the compressible model for all nodes. The approximations for the compressible fluid flow model are described in the next section.

2.3 Numerical Analysis of the Compressible Flow Model

There are several differences between the incompressible and compressible flow models. The major difference is that the density is not held constant in the compressible model and is allowed to vary as a function of pressure and temperature. The other major difference between the two models is that in the compressible flow case, the thrust chamber wall is modeled only as a single porous matrix system. Due to severe CPU run-time constraints, the compressible case was modeled as simple as possible. Therefore the porous liner section was not considered. Because the computational resources were limited to a PC, the run times for the compressible model were upwards of over one week to complete a single case study. This was due in large part to the very small time steps that were required to maintain the stability of the solution required in the explicit finite

difference scheme used. The requirement for the smaller time step in the compressible model as compared to the incompressible model is due to the inclusion of the transient terms in both the continuity and momentum equations used to solve for the fluid density and Darcy velocity respectively. In addition, the compressible model also uses the equation of state to determine the fluid pressure at the interior nodes.

The boundary conditions used at the coolant inlet boundary are constant temperature, pressure, and density. The Darcy velocity is determined from the momentum equation with the pressure gradient term being the driving force of the fluid. At this node, because the flow is in the negative r -direction, backward differencing is used in the pressure gradient term and the expression for the velocity is obtained as

$$u_n^{m+1} = \frac{1}{\rho_n^{m+1}} \left[\left(1 - \frac{\varepsilon_1 \Delta t}{\beta_1} |u_n^m| \right) \rho_n^m u_n^m - \frac{\varepsilon_1 \Delta t \mu_f}{\alpha_1} u_n^m - \frac{\varepsilon_1 \Delta t}{\Delta r} (P_n^m - P_{n-1}^m) \right] \quad (38)$$

The density, pressure, and temperature at the cold gas boundary come from the properties of the coolant as it enters the wall from the coolant reservoir and are implemented as boundary conditions. The development of the discretized equations for the compressible flow model described hereafter is provided in Appendix B.

The values for the variables in the interior nodes come from discretizing the governing equations. The solutions for the density, velocity, and pressure come from the continuity equation, momentum equation, and equation of state respectively. As is in the incompressible fluid flow model, the solution for the temperature comes from the energy equation, and since the energy equation in the incompressible model already incorporates

the transient term, the finite difference approximation of the temperature in the compressible flow model is exactly the same as it is for the incompressible flow model, or equation (34)

$$T_n^{m+1} = \left[\frac{\Delta t r_{n-1/2} k_A}{(\rho c_p)_A r_n \Delta r^2} + \frac{\Delta t \varepsilon_A \rho_n^m u_n^m c_{p_f}}{2(\rho c_p)_A \Delta r} \right] T_{n-1}^m + \left[1 - \frac{\Delta t (r_{n+1/2} + r_{n-1/2}) k_A}{(\rho c_p)_A r_n \Delta r^2} \right] T_n^m + \left[\frac{\Delta t r_{n+1/2} k_A}{(\rho c_p)_A r_n \Delta r^2} - \frac{\Delta t \varepsilon_A \rho_n^m u_n^m c_{p_f}}{2(\rho c_p)_A \Delta r} \right] T_{n+1}^m$$

For the density, the continuity equation was discretized using upwind differencing in the convective term. In this case, the flow is in the negative r -direction, so upwind differencing would involve the use of forward differencing. The fluid density for a typical interior node is

$$\rho_n^{m+1} = \left[1 + \frac{\Delta t u_n^m}{\varepsilon_A \Delta r} \right] \rho_n^m - \left[\frac{\Delta t r_{n+1} u_{n+1}^m}{\varepsilon_A r_n \Delta r} \right] \rho_{n+1}^m \quad (39)$$

For the Darcy velocity, the momentum equation was approximated using a backward difference method in the pressure gradient term because the flow is in the negative r -direction. The expression for the fluid velocity at any typical interior node takes the form

$$u_n^{m+1} = \frac{1}{\rho_n^{m+1}} \left[\left(1 - \frac{\varepsilon_A \Delta t}{\beta_A} |u_n^m| \right) \rho_n^m u_n^m - \frac{\varepsilon_A \Delta t \mu_f}{\alpha_A} u_n^m - \frac{\varepsilon_A \Delta t}{\Delta r} (P_n^m - P_{n-1}^m) \right] \quad (40)$$

The final variable needed to be solved for is the pressure, which comes from the solution of the equation of state. With the density and temperature already known, the pressure at a typical interior node is

$$P_n^{m+1} = \rho_n^{m+1} R_f T_n^{m+1} \quad (41)$$

The solution for the temperature at the hot gas boundary comes from the same energy balance used in the incompressible flow model and the equation to describe this relation is the same as equation (37)

$$T_1^{m+1} = -\frac{1}{3}T_3^{m+1} + \frac{4}{3}T_2^{m+1} - \left(\frac{2 \cdot \Delta r}{3 \cdot k_2}\right)q''$$

Another difference between the incompressible flow model and the compressible flow model with respect to the hot gas boundary is that in the compressible flow model a constant pressure is assumed. Using this pressure boundary condition together with the boundary temperature calculated from the energy balance, the equation of state can be arranged to solve for the fluid density at the hot gas boundary. As with the interior nodes and the cold gas boundary node, the momentum equation is used to solve for the Darcy velocity of the fluid at the hot gas boundary, however with a slight alteration. It is not possible to use backward differencing at the hot gas boundary node, so the pressure gradient is approximated using forward differencing at the hot gas boundary as shown in Appendix B.

2.4 Developing the Codes

To perform the calculations that are necessary to determine the behavior of the fluid and the temperature distribution throughout the thrust chamber wall, two FORTRAN programs were developed for the incompressible fluid flow and compressible fluid flow models. A flowchart that shows the method for writing the incompressible flow program and the compressible flow program are included in Appendix C and Appendix D respectively. The entire programs titled, INCOMP and COMP are included in Appendix E and Appendix F respectively. The programs for the different models are similar in

structure. Both programs consist of a main program followed by a series of function subroutines. The functions correspond to the equations needed to be solved for each of the parameters throughout the thrust chamber wall. For instance, the calculation for the temperature inside the porous foam in the incompressible model is defined inside the function called TFOAM. The main program for each model starts out very similar. First each of the parameters are initialized and then defined. The thermal properties of the coolant and porous matrices as well as the material properties of the porous matrices are input by the user. Three arrays are initialized and defined that represent the radial distance of each node. The first array represents the distance from the center of the chamber for each node in the array. The other two arrays correspond to the mid-point between the radial nodes that are used in the energy equation to solve for the temperature and are labeled RPLUS and RMINUS. At this point, the programs for the incompressible flow model and compressible flow model begin to differ.

In the incompressible flow model, the density is constant and defined, and the velocity and pressure are independent of the temperature. Therefore, the velocity and pressure arrays are set up and calculated first. The fluid travels in the negative r -direction beginning with the last node of the array, which corresponds to the cold gas boundary and is labeled as NTOT. The cold gas boundary pressure is kept constant. The velocity is determined from the specified inlet mass flow rate. After the cold gas boundary, the properties are calculated by calling the appropriate functions in the porous foam, followed by the interior interface boundary, porous liner, and hot gas boundary, in that order. After the pressure and velocity are calculated at each node an absolute tolerance

check is performed. The values at each node are compared to their corresponding values from the previous iteration. During the tolerance check, the value of the node with the greatest difference in value from the previous iteration is stored in a parameter called PEPS and UEPS corresponding to the pressure and velocity differences respectively. These maximum variations are then compared to the maximum allowable variations, MAXDP and MAXDU, which were specified to be 10^{-7} after a series of trials to determine how small the absolute differences could be without compromising the run time of the program. Once both PEPS and UEPS have a value less than their respective tolerance levels, the pressure and velocity distributions are stored and the iterations end and the calculation for the temperature begin. The set-up for the temperature at each node throughout the wall is very similar to the set-up for the calculation of the pressure and velocity. The only difference in the temperature calculations is the order in which the functions are called. The values in the porous foam and the porous liner are calculated before the temperature at the interior interface boundary is calculated. The same procedure previously described to check if the user defined tolerance is met for the pressure and velocity is used for the temperature array. Once the temperature array has met the tolerance levels, the values at each node for the pressure, velocity, and temperature are written into data files for importation into a spreadsheet for analysis.

In the compressible flow model, the density, pressure, velocity, and temperature must all be calculated at each node before they can be calculated at the next node. As in the incompressible model, the first calculations come at the cold gas boundary. Next are the calculations in the porous matrix, followed by the hot gas boundary. As previously stated

there is only one porous matrix in the compressible flow model. For the interior nodes however, the density must be calculated first because the derivation of the momentum equation calls for the use of the value of the density at both the current and previous time step. After the density is calculated, the velocity function is called, followed by the temperature function, then the equation of state is used to calculate the pressure. As in the incompressible model, a tolerance check is performed after the parameters at each node are calculated at each time step. Similar to the incompressible flow code there are tolerance checks implemented into the compressible flow code to determine whether the solution satisfies a user defined tolerance. In the code for the compressible code, all four variables have their own separate tolerance check. Once the tolerance conditions for all four variables are met, the values for the density, pressure, velocity, and temperature are written into data files for importation into a spreadsheet for analysis.

Chapter 3: Model Comparison and General Results

In this chapter, the results of the compressible and incompressible flow models for a single porous matrix are presented and compared. Before those results are presented, a study on how the grid sizing affects the numerical results is presented. Also presented are some general results that show how a transpiration cooled liquid rocket engine thermally responds to different coolant mass flow rates across the thrust chamber wall.

3.1 Grid Size Sensitivity Analysis

Before performing parametric studies on the transpiration cooled thrust chamber wall, it is necessary to determine how the grid size will affect the results. Due to CPU run time constraints, the incompressible model was used to perform this analysis. For this study the thrust chamber wall was given an inner radius of 15 cm and a thickness of 6 cm. The porosity of the material was chosen to be $\varepsilon = 0.50$ corresponding to the porosity of the porous foam, which is discussed in the next chapter. The pressure at the cold gas boundary was set at a constant value of 1.35 MPa. The inlet mass flow rate was set at 7.22 kg/s resulting in a hot gas boundary pressure of approximately 1.31 MPa. The simulation was run five times with a different number of nodes being used in each case. The number of grid points used was 31, 51, 71, 101, and 151. As the number of grid points increases, the results should become more accurate. Hence it can be assumed that the results for the test case using 151 grid points were the most accurate. Even though these numerical results are not being compared to actual data, it will be assumed that the results for the test case using 151 nodes are the most accurate. The purpose of this study is to determine how large the grid size can be before there is a significant difference in

the results. The results of the nodal analysis show that there is not a significant difference in the results obtained with a different number of nodes. Figure 3.1 shows the temperature distribution inside the chamber wall for the analysis run with varying grid

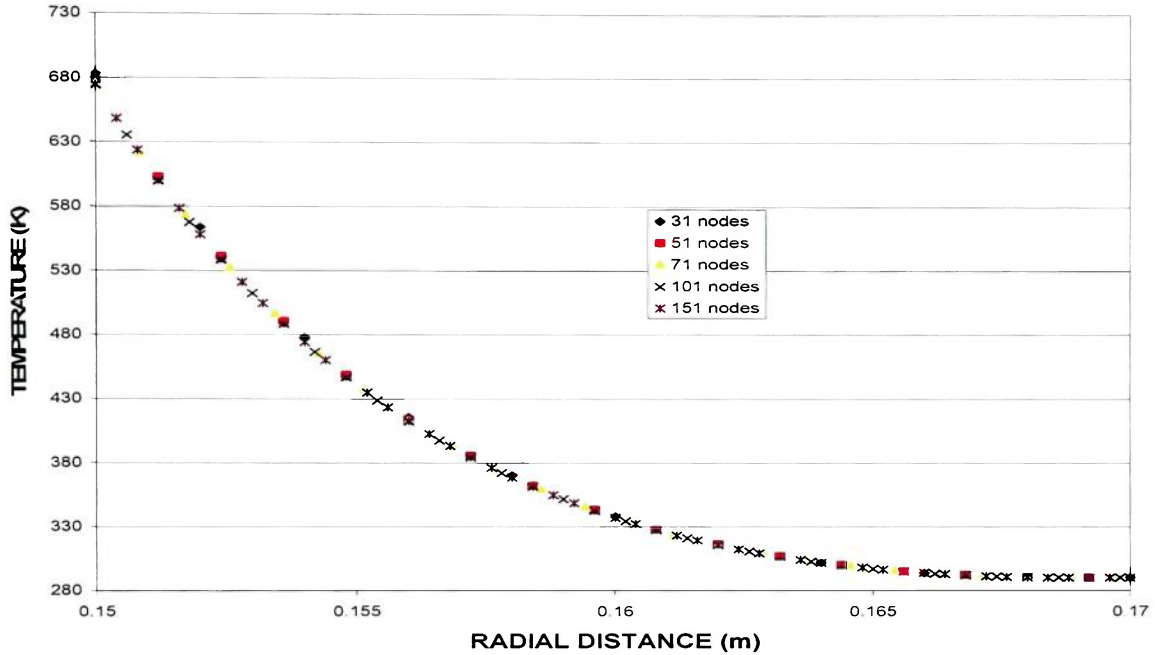


Figure 3.1: Temperature Distribution Results Using 5 Different Numbers of Nodes

sizes. It should be noted that the plots in Figure 3.1 do not represent the entire thickness of the thrust chamber wall. When the radial distance is larger than 16.8 cm, the temperature remains practically at a constant 290 K, equal to the inlet temperature at the cold gas boundary, in all cases. This data is omitted to allow for a closer look at the

# of Nodes	HGB Temperature (K)	Relative Difference
31	682.991	1.26%
51	677.683	0.47%
71	675.986	0.22%
101	674.190	0.05%

Table 3.1: Relative Temperature Difference at the Hot Gas Boundary for Varying Grid Spaces Compared to the HGB Temperature Using 151 Nodes

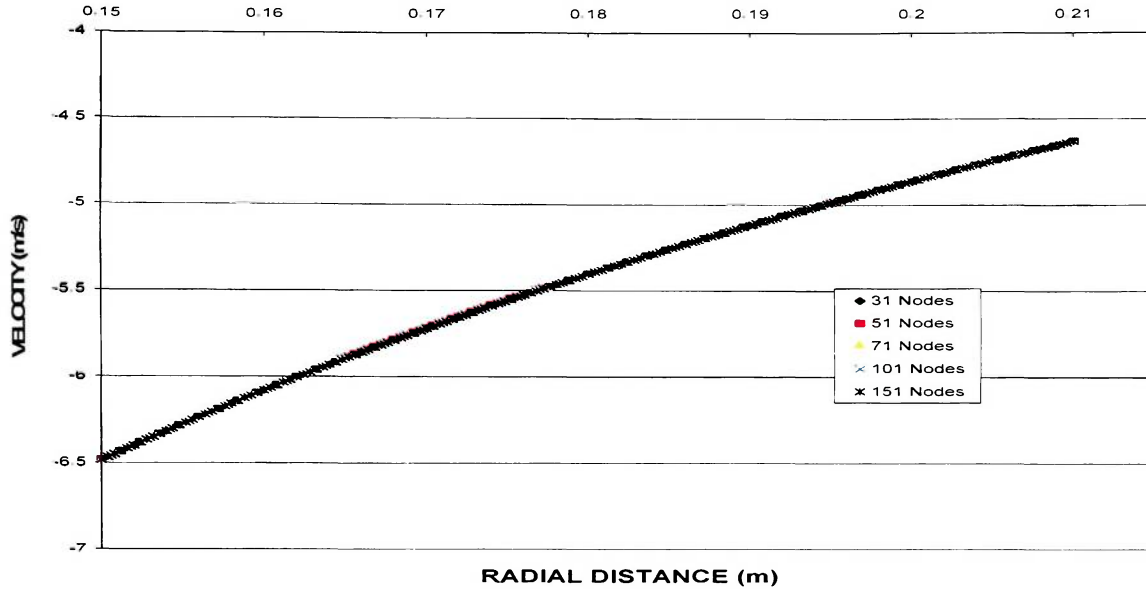


Figure 3.2: Velocity Distribution Results Using 5 Different Numbers of Nodes

points where there is a detectable temperature difference. It is difficult to determine if there is any difference in temperature between the cases from the plots just through observation. The value of the temperature at the hot gas boundary in the case where 151 grid points are used is 674.496 K. Table 3.1 shows the hot gas boundary temperatures of the other four cases as well as their relative differences with respect to the 151 node case. For further analysis, Figure 3.2 and Figure 3.3 show the velocity and pressure distributions respectively for varying grid sizes. Similar to the temperature distribution, it is difficult to determine the differences in pressures and velocities from their respective

# of Nodes	HGB Velocity (m/s)	Relative Difference
31	-6.4840	0.0014%
51	-6.4835	0.0096%
71	-6.4842	0.0011%
101	-6.4841	0.0004%
151	-6.4841	0.0000%

Table 3.2: Relative Velocity Difference at the Hot Gas Boundary for Varying Grid Spaces

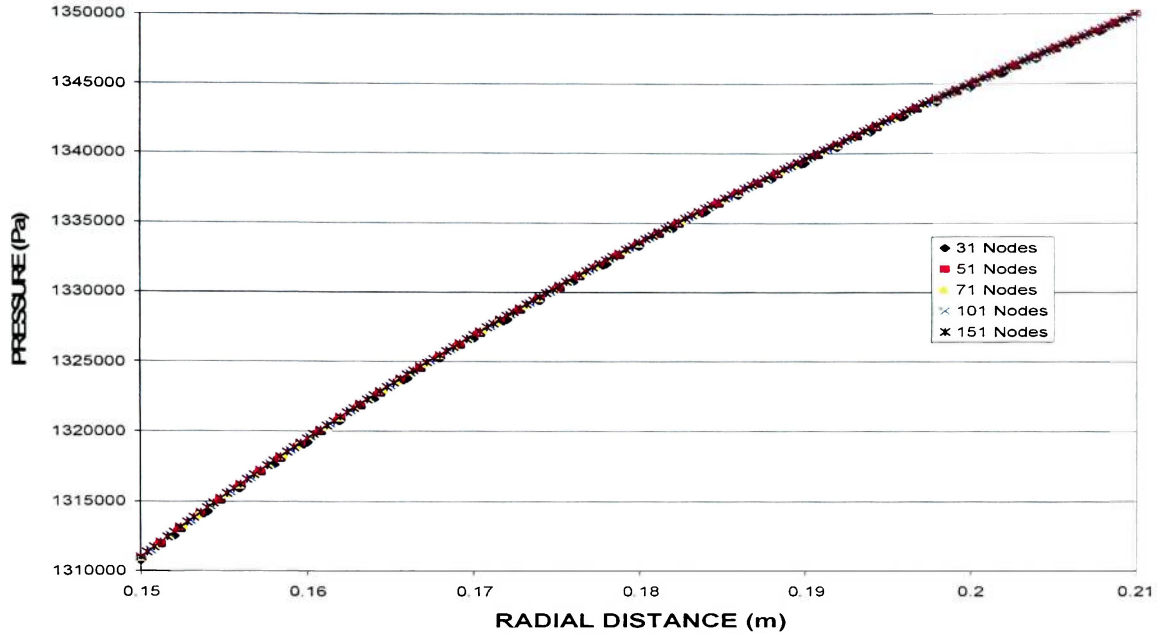


Figure 3.3: Pressure Distribution Results Using 5 Different Numbers of Nodes

plots. As is in the case with the temperature distributions, the greatest difference in velocity and pressure occurs at the hot gas boundary. Table 3.2 and Table 3.3 show the hot gas boundary pressures and velocities and compare them to their respective values when using the 151 node simulation. The results for the pressure and velocity comparisons show that the grid size has an insignificant effect on the values of these two variables. In general, the number of grid points has only minimal effects on the accuracy

# of Nodes	HGB Pressure (Pa)	Relative Difference
31	1310744	0.0222%
51	1310896	0.0106%
71	1310953	0.0063%
101	1310998	0.0028%
151	1311035	0.0000%

Table 3.3: Relative Pressure Difference at the Hot Gas Boundary for Varying Grid Spaces

of the final results when compared to the case where 151 nodes were used. This was verified from the maximum relative differences that resulted for each of the three variable profiles. When a grid size of 51 nodes or larger was used, the maximum relative temperature difference did not exceed 0.50% and the maximum relative pressure or Darcy velocity difference did not exceed 0.01%. When performing the parametric studies, it is best to use the smallest number of grid points that is acceptable in order to minimize the CPU time for each analysis. The results of this nodal analysis show that it would be acceptable to use 51 grid points to perform the parametric studies. In the parametric studies the thickness of the porous liner section was a fraction of the thickness of the porous foam section. Therefore if 31 total grid points were used; there would not be a sufficient number of grid points to represent the porous liner section to produce sufficiently accurate results for this section. For this reason, it was also necessary to increase the overall number of grid points when looking at a porous liner section that represents only 10% of the thrust chamber wall thickness.

3.2 General Results

Transpiration cooling uses a portion of a rocket's propellant as a means of cooling the thrust chamber wall. As the propellant flow increases inside the wall, the temperature of the wall decreases. The following results were obtained when using a liner that has a thickness that represents 20% of the total thrust chamber wall thickness and has a porosity of 0.25. A hot gas boundary heat flux of $30,000 \text{ W/m}^2$ was applied in each of the cases. The porosity of the foam section was 0.50. The results in Figure 3.4 confirm that as the inlet coolant mass flow rate increases, the temperature throughout the wall

decreases. The inlet mass flow rate also affects the velocity of the fluid inside the wall as well as the pressure drop across the wall. Figure 3.5 shows how varying the inlet mass flow rate affects the pressure distribution and the overall pressure drop across the wall.

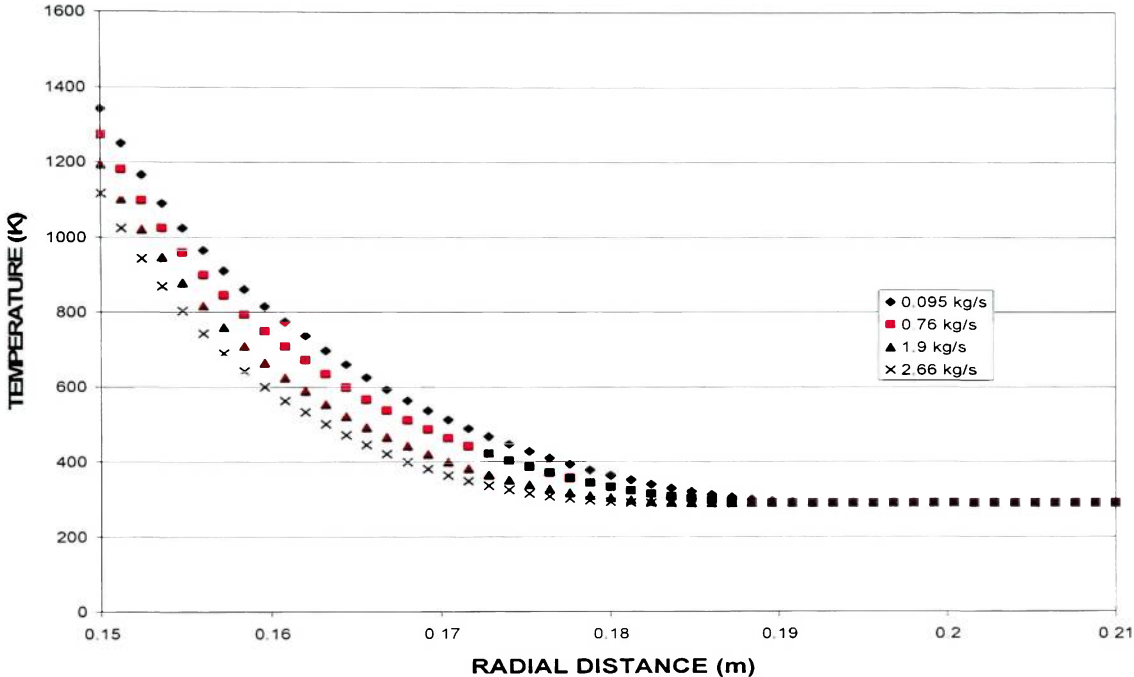


Figure 3.4: The Effects of Different Inlet Mass Flow Rates on the Temperature Distribution Across the Thickness of the Wall

There is a much larger pressure drop in the porous liner section compared to the porous foam section. This is due to a lower permeability because of lower porosity of the liner, which requires a larger pressure drop. The results show that as the pressure drop across the entire thickness of the wall increases, the inlet mass flow rate increases. The pressure drop must remain below a certain threshold in order for the hydrogen to remain in supercritical state. This constraint limits the amount of propellant that can be used as coolant. The effect of the inlet mass flow rate on the Darcy velocity of the fluid is shown in Figure 3.6. As the mass flow rate increases the Darcy velocity increases naturally. The results of Figure 3.6 also show that as the mass flow rate increases, the difference in

velocity from the cold gas boundary to the hot gas boundary increases. The increase in mass flow rate produces an increase in the Darcy velocity of the fluid throughout the wall. The pressure drop of the coolant across the wall has the greatest effect on the temperature distribution of the coolant and the thrust chamber wall. The porosity of the

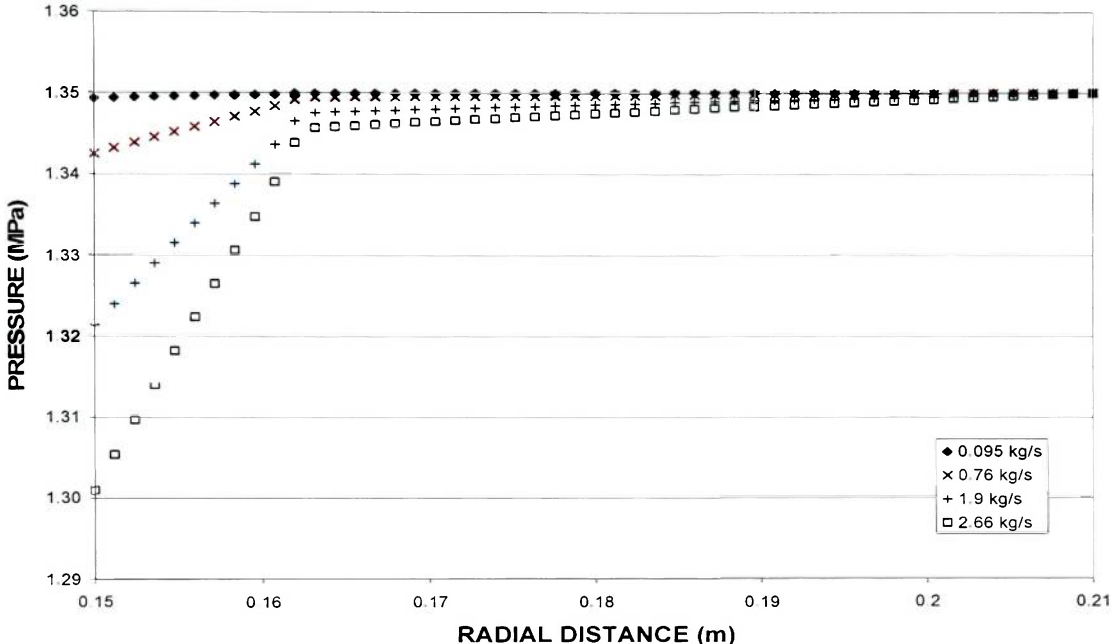


Figure 3.5: The Effects of Different Inlet Mass Flow Rates on the Pressure Distribution Across the Thickness of the Wall

porous liner is smaller than in the porous foam causing a lower permeability in the porous liner section, which requires a larger pressure drop in this section. An increase in the mass flow rate comes with the penalty of a larger required pressure differential across the entire thickness of the thrust chamber wall. The increase in the inlet mass flow rate increases the speed of the fluid flow inside the thrust chamber wall, which increases the mass flow rate of the coolant inside the wall. The increase in mass flow rate also corresponds to an increase in the mass of coolant that is inside the thrust chamber wall. The coolant, along with the porous matrices absorbs the energy produced from the

combustion products. The temperature increase inside the thrust chamber wall gets smaller as more coolant is introduced into the wall.

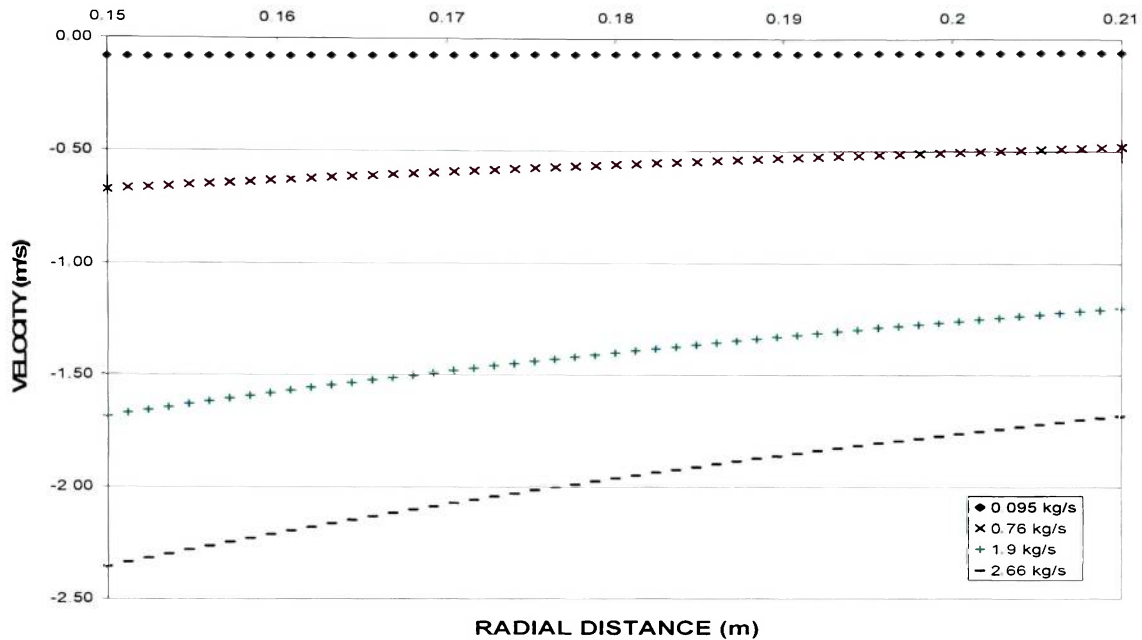


Figure 3.6: The Effects of Different Inlet Mass Flow Rates on the Velocity Distribution Across the Thickness of the Wall

3.3 Comparing the Results from the Two Models

Due to stability issues with the explicit finite difference scheme, a very small time step is required to obtain results using the compressible flow model. This has rendered the computational time prohibitively extensive for the compressible flow model with the available computational resources. For this reason, the incompressible model is the only model used for performing the parametric studies desired for this research. In order for the incompressible model to be used as a reliable tool for the parametric studies an investigation was performed comparing the incompressible model results to the compressible model results for a test case. This section compares the results for the incompressible model to the results for the compressible model for a case of similar

conditions. For the test case, each model is given a cold gas boundary pressure of 1.35 MPa with a temperature of 290 K. As described in Chapter 2, the equation of state was used to calculate the density at the cold gas boundary in the compressible flow model. To ensure that the models have as similar conditions as possible, the value for the density of the incompressible model will be the same as the cold gas boundary density calculated in the incompressible model for all of the nodes in the incompressible model. The compressible model was given a hot gas boundary pressure of 1.31 MPa. In the incompressible fluid flow model the pressure at the hot gas boundary is determined from numerical analysis and is not user specified. Through a process of trial and error, a hot gas boundary pressure of approximately 1310 kPa is achieved when the mass flow rate at the inlet is 7.22 kg/s in this model. These values make up all of the given conditions necessary to make a comparison of the two models. For the models, a total of 51 grid points are used.

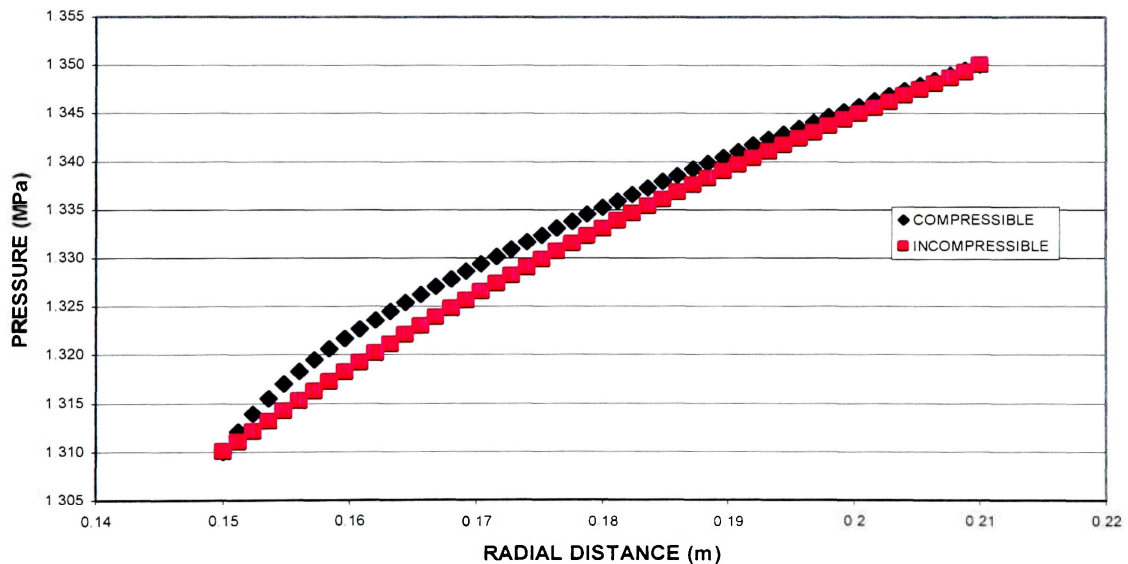


Figure 3.7: Pressure Comparison between the Two Models

Since the pressures at the boundaries in each model are the same, the first comparison between the two models will be between the pressure distributions throughout the wall thickness. It should be noted, that even though the pressures at the boundaries are the same, there is no guarantee that the mass flow rates will be similar. For the incompressible model to be considered an acceptable model for the parametric studies, it has to produce a similar temperature profile as the compressible model for a similar mass flow rate. The results for the pressure distribution for the two models are shown in Figure 3.7. The pressure distribution resulting from the incompressible flow model is slightly more linear than the pressure distribution resulting from the compressible flow model. The density and Darcy velocity distributions for the two models show significant differences however. By definition, the density is assumed constant in the incompressible flow model. For this reason, it would not be beneficial to look at the density comparison alone, which is shown in Figure 3.8. The density multiplied by the

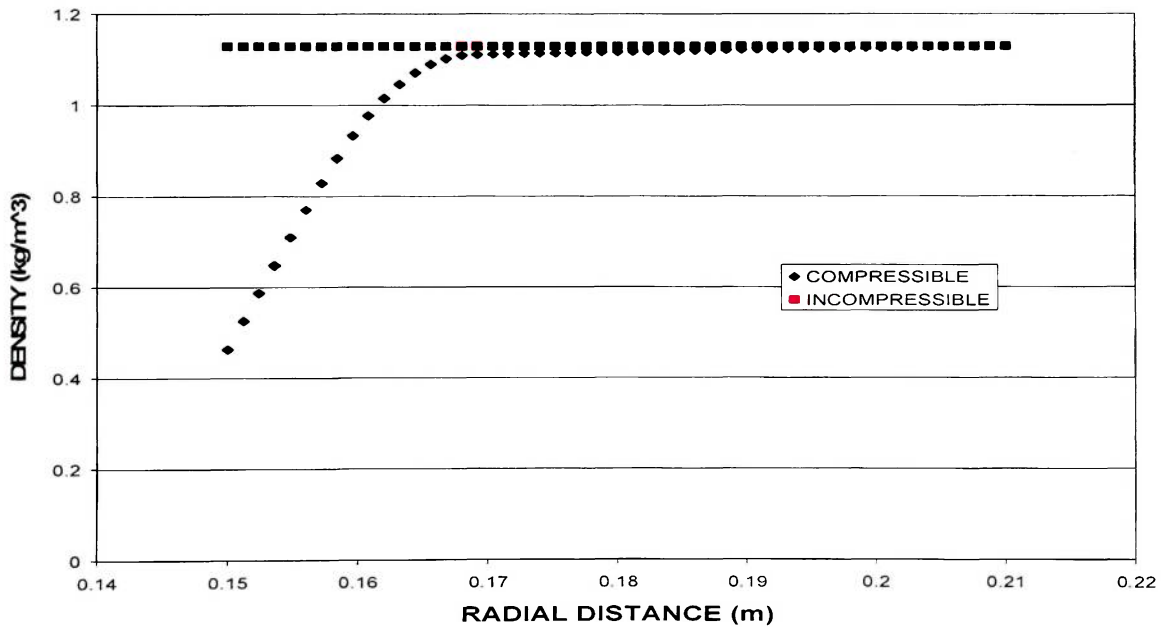


Figure 3.8: Density Comparison between the Two Models

Darcy velocity and cross-sectional area will produce the mass flow rate of the coolant at each node and therefore through each cross-section. It is the mass flow rate that will give an indication of whether the temperature distributions can be expected to be similar. Near the cold gas side, the density remains fairly constant, showing only minor decreases as the fluid flows toward the hot gas side. This initial small decrease corresponds to the nodes in the wall where the temperature is constant as shown later in Figure 3.11. When the temperature begins to rise, the density sharply decreases. With the pressures nearly similar, the continuity equation should counter the sharp decrease in density with an increase in the magnitude of the velocity. While the magnitude of the Darcy velocity does increase from the cold gas boundary to the hot gas boundary in the incompressible model, there is a significantly greater change in the velocity distribution in the compressible flow model as shown in Figure 3.9. As the fluid nears the hot gas

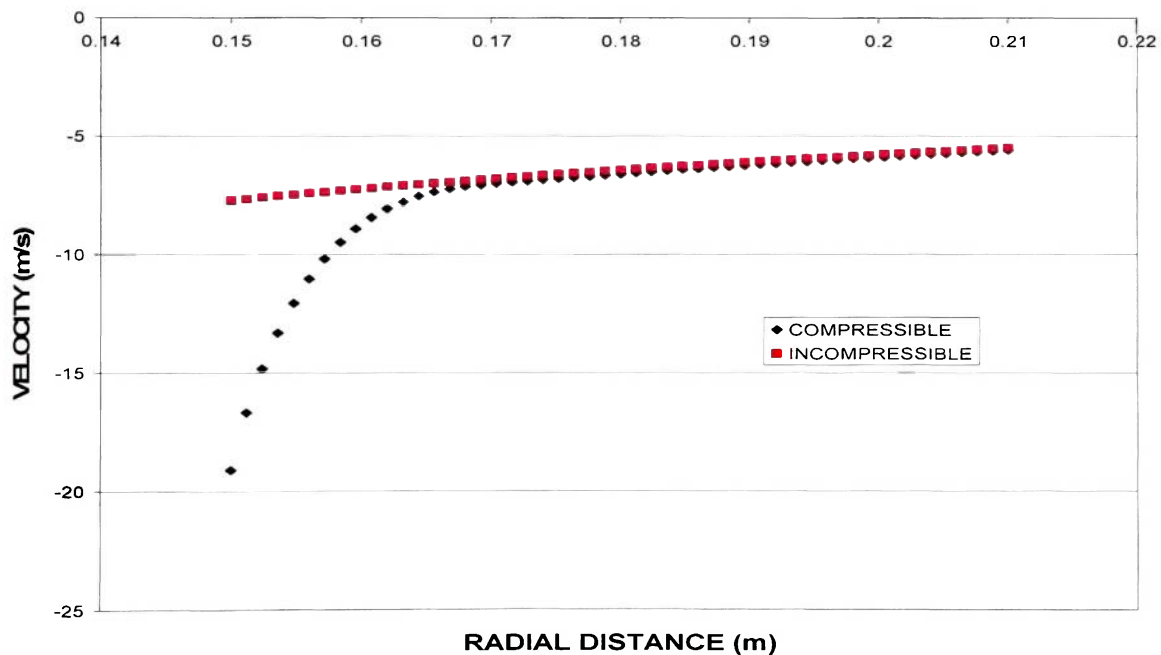


Figure 3.9: Velocity Comparison between the Two Models

boundary, the Darcy velocity increases in the negative r-direction. The Darcy velocity increases in magnitude linearly at the nodes where the temperatures remain constant as the cross-sectional area decreases linearly in the negative r-direction. Before the temperature increases, the velocity distribution for the incompressible model shows similar behavior to the compressible flow model. When the temperature increase, however, the speed of the fluid in the compressible flow model begins to significantly increase while the incompressible model speeds continue to increase at their previous

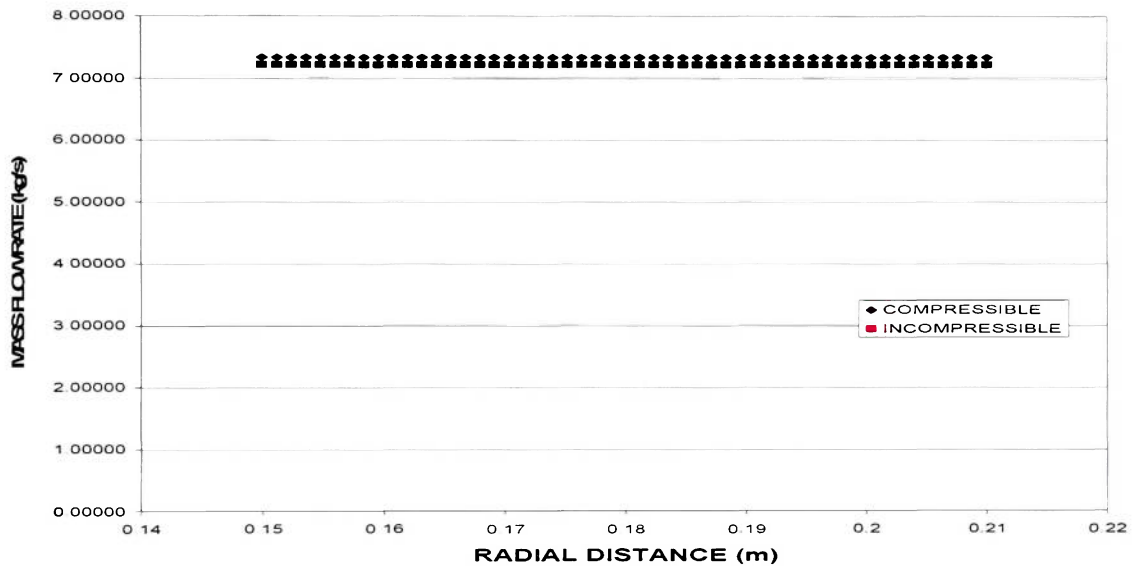


Figure 3.10: Comparison of the Mass Flow Rate for the Two Models

rate. At first glance, the results of Figures 3.8 and 3.9 would make it seem that the incompressible flow model would not make a realistic model for the fluid flow behavior. However, when the results of these two comparisons are combined, they provide evidence that the incompressible flow model is useful. When the fluid density is multiplied by the magnitude of the Darcy velocity and the area, the result is the mass flow rate of the fluid at each nodal cross-section. If the mass flow rates of the two models are similar, then it is expected that the temperature distributions of the two

models will also be similar. This can be followed from the energy equation. In the energy equation the convective term involves the product of the fluid density and the Darcy velocity. The mass flow rates of each model are displayed in Figure 3.10. The mass flow rates for the two models are constant which signifies that the solution has reached steady state. The compressible flow model has a mass flow rate of 7.34 kg/s while the incompressible model has a mass flow rate of 7.22 kg/s. There is a 1.6%

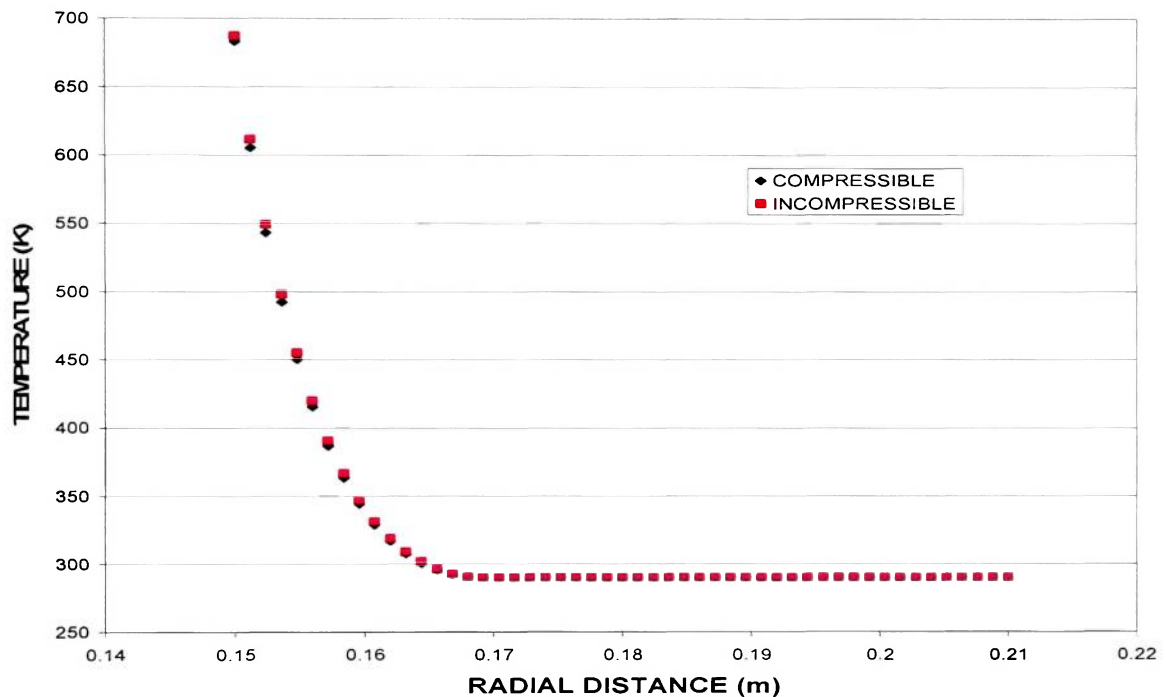


Figure 3.11: Temperature Comparison for the Two Models

difference in the mass flow rates with the compressible flow model having the slightly larger mass flow rate at each node. The similar mass flow rates were obtained through a trial and error process involving adjusting the boundary conditions, specifically the mass flow rate from the coolant reservoir. The relatively small difference along with the similar distribution of the mass flow rates of the two models should provide a similar temperature distribution between the models. The comparison of the temperature

distribution is shown in Figure 3.11. As expected, the temperature distribution between the models is similar. The magnitude of the temperature difference increases as the flow approaches the hot gas boundary with the maximum temperature occurring at the hot gas boundary. Since the mass flow rate of the compressible flow model was slightly larger, it is not surprising that the maximum temperature in the compressible model is slightly smaller than that of the incompressible model. This can be explained by slightly more coolant being present in the porous matrix yielding a slightly higher effective thermal conductivity as well as slightly increased magnitude of the advection term in the energy equation. The temperature at the boundary for the compressible model is 683.1 K while the incompressible model temperature is 686.9 K, a difference of only 0.5%. The first temperature difference between the two models occurs at node 16 with the difference being only 0.08%.

Because the density is held constant in the incompressible model, it was expected that the density and velocity distributions for the two models would have significant differences. However the similarities in the mass flow rate and temperature distributions show that the incompressible model can be used as an acceptable tool for determining the temperature distribution and the maximum temperature inside the thrust chamber wall to a very good accuracy level.

Chapter 4: Parametric Studies

In Chapter 3 it was shown that the computer programs numerically simulated the steady-state effects for the profiles of the variables defined by the governing equations and boundary conditions for a transpiration cooled liquid rocket engine. In this chapter, the previously defined governing equations and boundary conditions used to define the incompressible flow model will be used to perform parametric studies on the porous liner section. Two different test cases were analyzed. The first study looks at how the change in the porosity of the liner section affects the fluid flow and the second study looks at how varying the thickness of the liner section affects the fluid flow and temperature distribution across the thickness of the thrust chamber wall.

4.1 Basic Test Parameters

Some of the parameters remain constant for all of the test cases that are performed. The radius of the thrust chamber was chosen to be 15.0 cm with the thrust chamber wall having a thickness of 6.0 cm. The material used for both of the porous matrices is Silicon Carbide, Si-C, a ceramic-matrix-composite (CMC) being developed by Ultramet in conjunction with research at the Air Force Research Laboratory (AFRL). The properties used in this analysis come from the Ultramet website, www.ultramet.com, as well as a publication of Ultramet researchers (Brockemeyer 1998). The density, thermal conductivity and specific heat of Si-C are common throughout each case and are used for both the porous foam and the porous liner. The density is 3200 kg/m^3 , the thermal conductivity is 1.0 W/(mK) and the specific heat is 1422.6 J/(kg K) . The porosity, or

void fraction, and the mean pore diameter of the porous foam section are also constant for all test cases with the porosity being set at 0.50 and the mean pore diameter is 0.635 mm. The porosity and mean pore diameter are used to determine the permeability coefficients found in the momentum equation.

All of the thermophysical properties for the coolant fluid remain constant for each of the cases tested. The coolant is supercritical hydrogen and the parameters used come from the NIST website, www.nist.gov, mentioned in Chapter 1. Since the properties of hydrogen were not available for the complete range of temperatures that occur in this study, the properties are assumed to remain constant throughout these investigations. The properties for hydrogen used in this study are shown in Table 4.1. Since the incompressible flow model is being used, the density remains constant for all nodes throughout the wall.

Property	Value	Units
Thermal Conductivity	0.20	W/(m.K)
Viscosity	8.60×10^{-6}	kg/(m.s)
Specific Heat	14.70	J/(kg.K)
Density	1.20	kg/m ³

Table 4.1: Hydrogen Properties

4.2 Effects of Varying Porous Liner Thickness

One of the objectives of this thesis was to analyze how the addition of a porous liner to the porous foam affects the temperature distribution as well as the flow rate of the coolant throughout the thrust chamber wall. The first of the two main cases is to study how the coolant behavior changes when the thickness of the porous liner is varied. In this study the wall is modeled with porous liner section comprising 10%, 20%, and 30% of the total thrust chamber wall thickness. The results of these studies are also compared to the single layer case where no porous liner is used. For these studies the physical and thermal properties of both the porous foam and porous liner remain constant and are listed in Table 4.2. For each of the cases, the inlet mass flow rate and hot gas boundary heat flux are the varying parameters. For these studies, a mass flow rate is specified and then simulations are run varying the hot gas boundary heat flux. The heat flux is varied until the maximum allowable heat flux is reached. The maximum heat flux is determined by the maximum temperature that the porous matrices can withstand. The porous Si-C used in this study has a maximum allowable temperature of 1500 K. For a given inlet mass flow rate, simulations were run with different hot gas side heat fluxes until it was

Property	Foam Value	Liner Value	Units
Porosity	0.5	0.25	
Pore Diameter	6.35×10^{-4}	3.54×10^{-4}	m
Thermal Conductivity	0.1	0.45	W/(m.K)
Specific Heat	1422.6	1422.6	J/(kg.K)
Density	3200.0	3200.0	kg/m ³

Table 4.2: Properties of the Porous Foam and Liner for the Varying Thickness Analysis

determined which heat flux would provide a maximum temperature inside the thrust chamber wall of 1500 K. The maximum temperatures occur at the hot gas boundary in every case. Since the system is being modeled assuming local thermal equilibrium, the temperature of the coolant fluid also represents the temperature of the porous matrix. Each case begins with a specified mass flow rate of 0.048 kg/s with the mass flow rate increasing until the maximum allowable heat flux is found. The inlet mass flow rate is bounded by the pressure drop across the thrust chamber wall. Each of the test cases has a different maximum inlet mass flow rate. A total of 51 nodes are used for the cases where the liner is 20% and 30% of the total thickness as well as the case where no liner is used. For the case where the liner is 10% of the total wall thickness, using 51 nodes leaves only 5 nodes to represent the porous liner. Therefore a total of 101 nodes are used for the uniform grid size leaving 10 nodes for the porous liner section.

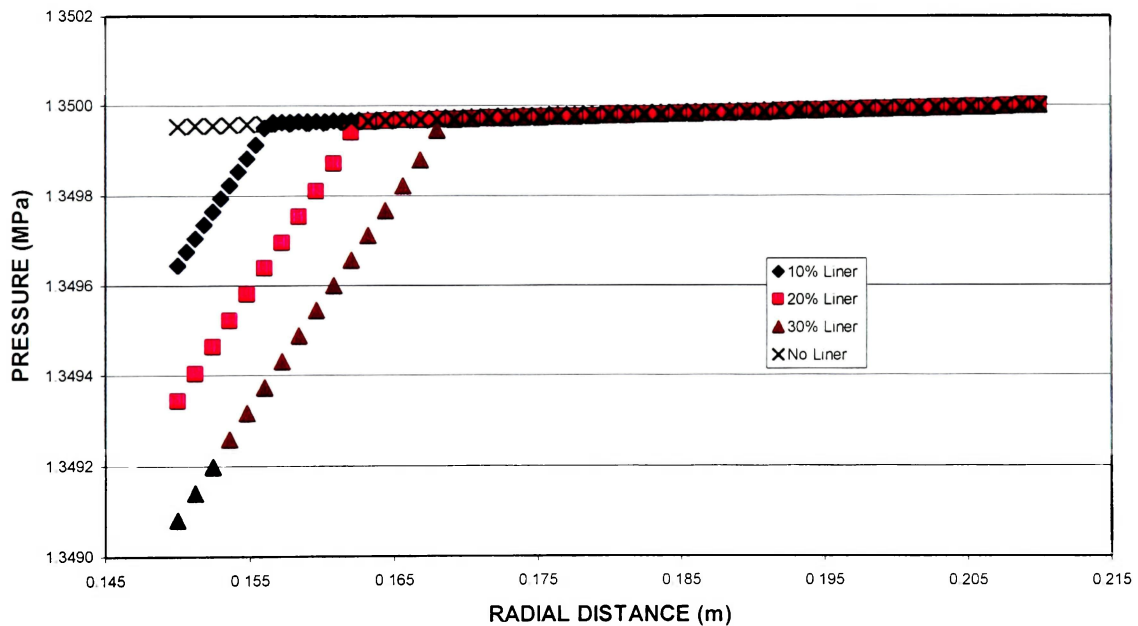


Figure 4.1: Typical Pressure Distribution for Varying Liner Thickness

One of the previously mentioned constraints is that the pressure remains above 1.30 MPa at all points inside the thrust chamber wall. The typical pressure distributions inside the wall for the four different cases are shown in Figure 4.1, where a heat flux of 30,000 W/m² and an inlet mass flow rate of 0.095 kg/s are constant throughout the 4 cases. The results of Figure 4.1 show that as the thickness of the liner increases, a larger pressure drop is required for a specified inlet mass flow rate. Since there is a difference in pressure drop under the same conditions for the various liner thickness cases, there is a difference in the range of inlet mass flow rates that can be used without causing the pressure drop to become too large. The maximum inlet mass flow rates for each case are shown in Table 4.3. The maximum inlet mass flow rates in Table 4.3 are the inlet mass flow rates for each of the test cases that are required when there is a total pressure drop of 50 kPa across the thrust chamber wall. Simulations for each case were performed with

Liner Thickness	Maximum Mass Flow Rate (kg/s)
10%	4.00
20%	2.66
30%	2.09
No Liner	8.17

Table 4.3: Maximum Mass Flow Rate for Varying Liner Thickness

the inlet mass flow rate ranging from a minimum value of 0.095 kg/s up to 1.9 kg/s for a comparison of the coolant behavior at the various liner thicknesses. Figure 4.2 shows how the pressure drop varies as the inlet mass flow rate increases for each of the test cases. The greatest pressure drops occur when the liner section has a thickness of 30% of the total thickness of the thrust chamber wall, while the smallest pressure drops occur when no liner is used over the given range of inlet mass flow rates. These results were

expected. One of the purposes of the liner might be to control the flow of the fluid inside the wall. Of course, the liner also provides structural integrity to the thrust chamber wall. The porous liner has a lower porosity than the porous foam. Therefore it has different permeability coefficients and a different effective thermal conductivity. As the thickness of the liner increases, there should be a greater effect on the behavior of the coolant flow and the temperature of the system. The pressure drop distribution for the three test cases where a liner was used is very similar as far as their rate of increase as the inlet mass flow rate increases. The difference between the cases is the magnitude of the pressure drop.

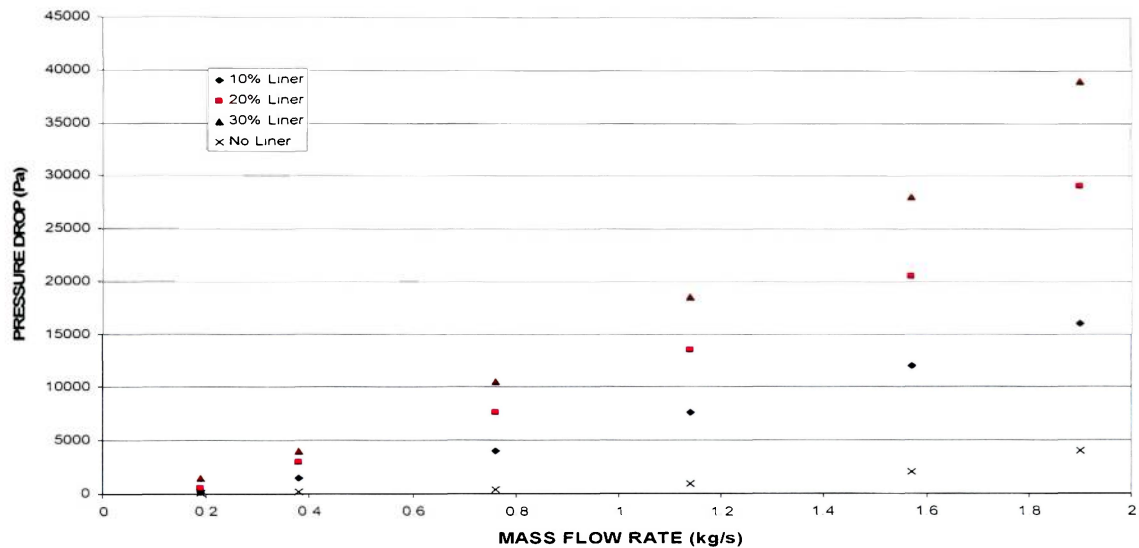


Figure 4.2: Pressure Drop Comparison for the Varying Liner Thickness

Similar to the case presented with the pressure distributions for each of the test cases, Figure 4.3 shows the temperature distribution of each of the four cases with an inlet mass flow rate of 0.095 kg/s and a hot gas boundary heat flux of 30,000 W/m². For this case, using a liner that represents 30% of the overall wall thickness provides the lowest temperatures at each of the nodes inside the wall, with a 20% liner providing the next lowest temperatures, followed by the case where no liner is used then a 10% liner. This

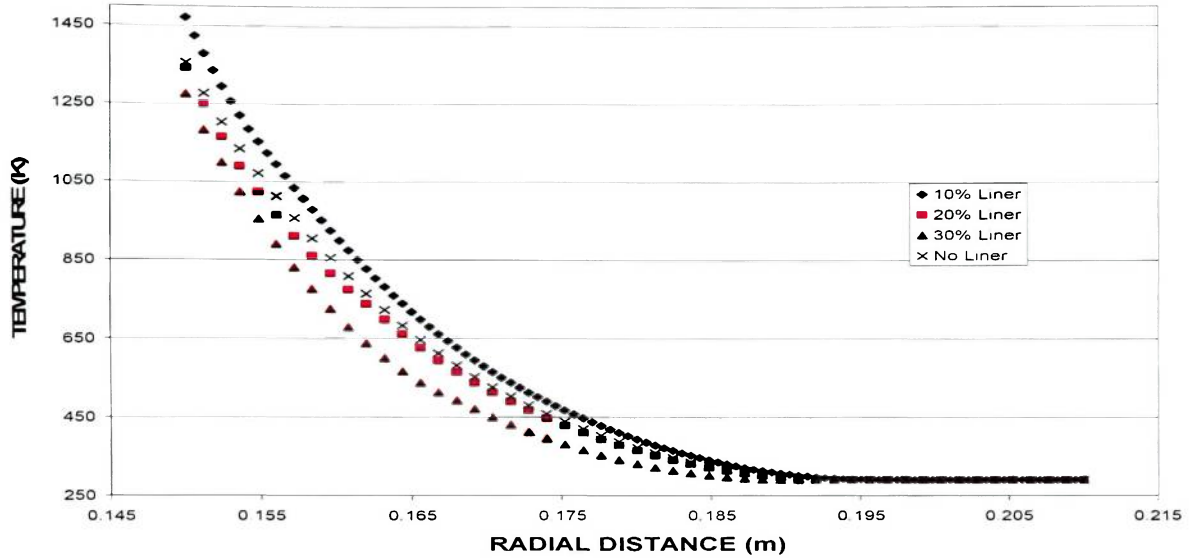


Figure 4.3: Temperature Distributions for the four cases with a 0.095 kg/s Inlet Mass Flow Rate and a 30,000 W/m² Heat Flux

does not hold true for all cases though. Figure 4.4 shows the temperature distributions for an inlet mass flow rate of 0.76 kg/s and hot gas heat flux of 30,000 W/m². In this case the 30% liner thickness case still provides the most efficient cooling method, however the case where a single porous matrix is used is now more efficient than the 20% liner

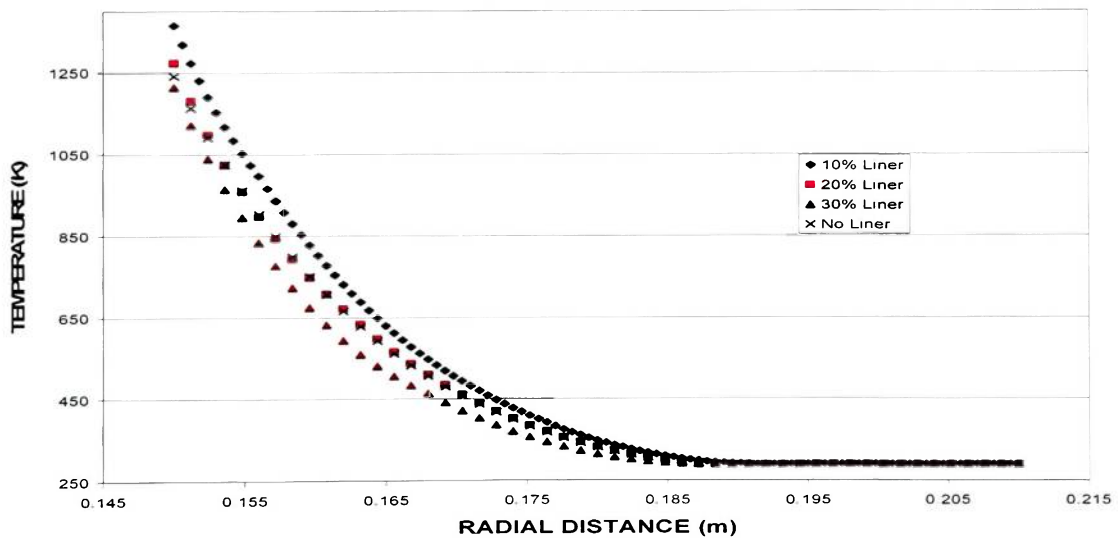


Figure 4.4: Temperature Distributions for the four cases with a 0.76 kg/s Inlet Mass Flow Rate and a 30,000 W/m² Heat Flux

thickness case. As the inlet mass flow rate increases the single porous matrix case becomes the most cooling efficient option as shown in Figure 4.5. In this case an inlet mass flow rate of 1.52 kg/s is used along with the 30,000 W/m² hot gas boundary heat flux. These temperature distributions show that there is no general behavior for the cases that were studied as the pressure drop and inlet mass flow rate are varied when comparing the temperature distribution between a thrust chamber wall with a liner and a thrust chamber wall without a liner. However in all of the simulations that were performed, the 30% liner thickness case provided the lowest hot gas boundary temperature compared to the other cases where a porous liner was used given the same

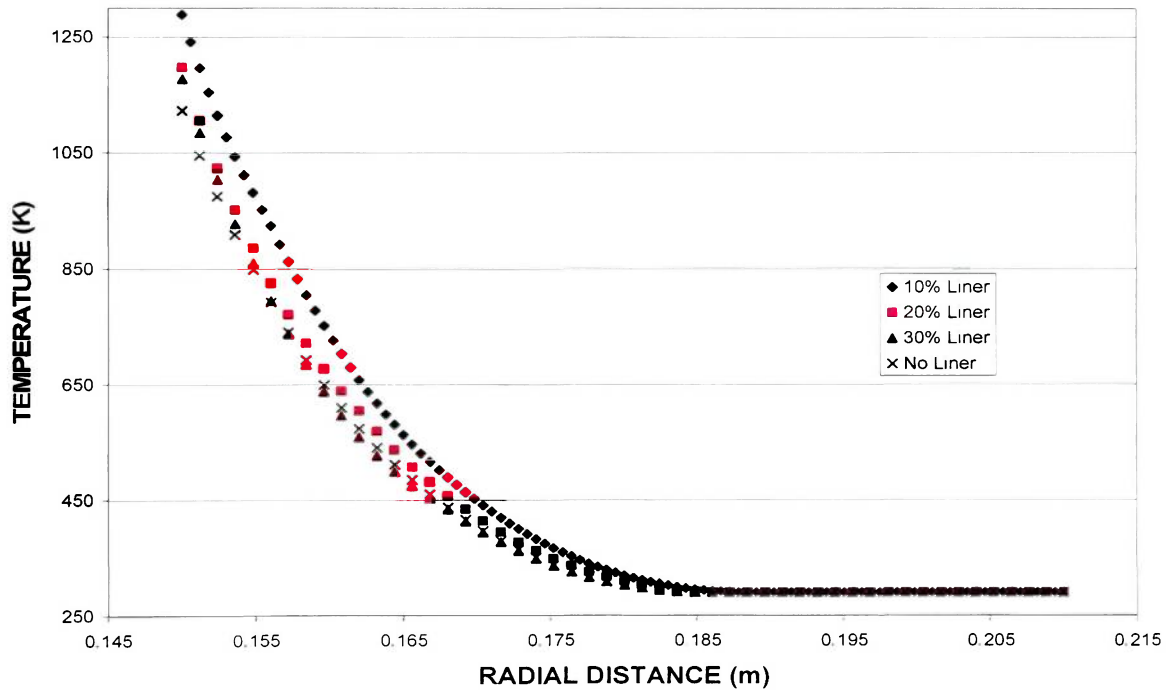


Figure 4.5: Temperature Distributions for the four cases with a 1.52 kg/s Inlet Mass Flow Rate and a 30,000 W/m² Heat Flux

inlet mass flow rate and hot gas boundary heat flux. It seems that there is no general trend in these three cases other than the fact that as the thickness of the porous liner

increases, the lower the temperatures become throughout the entire thickness of the wall when a porous liner is used. This is due in part to the effective thermal conductivity of the porous liner/coolant system. The porous liner has a lower porosity than the porous foam. Therefore there is a larger effective thermal conductivity of the porous matrix and coolant system when calculated using equation (10). This difference in the effective thermal conductivity between the porous foam section and the porous liner section is the reason that there is a difference in the temperature distribution between the cases where a porous liner was used and when just the porous foam was used. The larger effective thermal conductivity allows the liner to conduct the heat towards the porous foam at a better rate. The results in Figures 4.3, 4.4, and 4.5, show that the temperature remains at

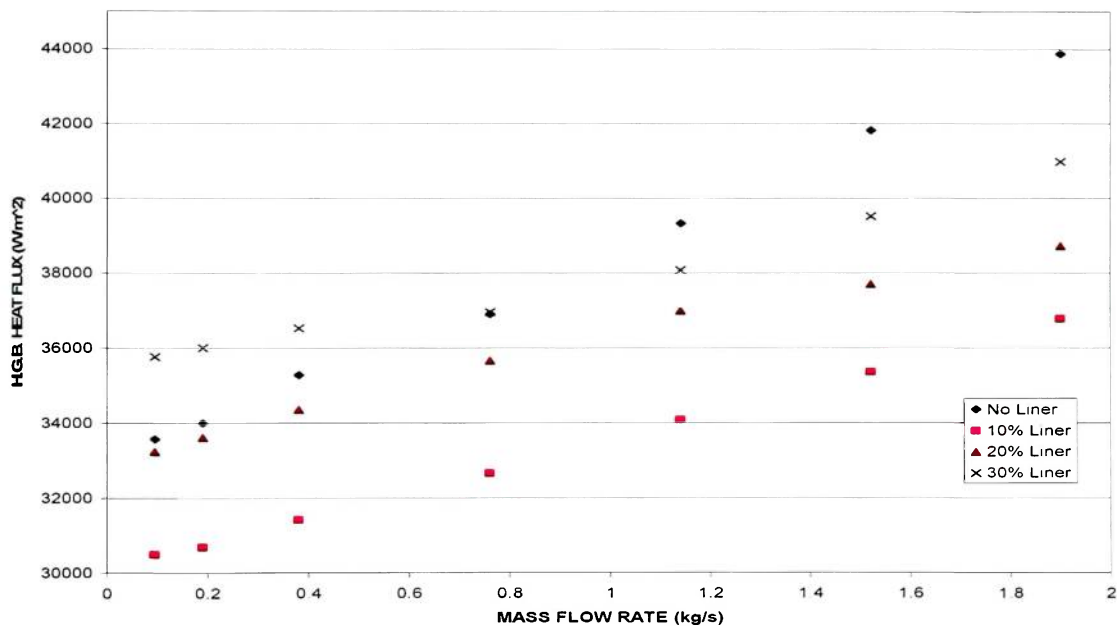


Figure 4.6: Maximum Heat Flux for the Different Liner Thickness Cases for Varying Mass Flow Rates

the cold gas boundary temperature of 290 K at radial distances greater than 0.185 m. The heat flux for a rocket engine will be determined by several factors including the type and

mixture of propellants and will not necessarily be $30,000 \text{ W/m}^2$. In order to try to obtain more general results, simulations were run for each of the test cases to see what the maximum allowable heat flux would be for various inlet mass flow rates. Again, the maximum allowable heat flux in this case is defined as the largest heat flux that does not cause the temperature at any point inside the thrust chamber wall to rise above the material failure limit, which in this case is 1500 K . As expected, the maximum allowable heat flux increases for each of the cases as the inlet mass flow rate increases. Figure 4.6 shows the distribution of the maximum allowable heat fluxes for the different test cases with varying inlet mass flow rates. Using the properties of Si-C provided by Ultramet, a 30% liner thickness system allows a larger maximum heat flux at mass flow rates of 0.76 kg/s or smaller. The single porous matrix case allows a larger maximum heat flux at inlet mass flow rates of greater than 0.76 kg/s . There was not a single case that was studied in which a liner that represents 10% of the total wall thickness provided a lower temperature distribution than the single porous matrix case. This study shows that there are cases where a thrust chamber wall consisting of two porous matrices can provide an overall lower temperature distribution across the thrust chamber wall when compared to a case where only a refractory porous foam is used.

4.3 Effects of Varying the Porosity of the Porous Liner

The researchers at Ultramet state that they are able to fabricate the Si-C used in their transpiration cooling tests at different porosities. This information allows for a second study to go along with the liner thickness study. In this section, the effects of varying the porosity of the porous liner section only are studied. For this study, the material

properties of the porous matrices as well as the hydrogen are the same as they were in the previous studies. For consistency, the porous liner section was chosen to represent 20% of the total thickness of the thrust chamber wall for each of the three porosity test cases. Simulations were run with the porous liner section having a porosity of 0.20, 0.25, and 0.30. By varying the porosity, the effective thermal conductivity as well as the permeability coefficients for the porous liner section were affected. The pressure and temperature constraints discussed in section 4.2 remain in effect. The pressure of the hydrogen is not allowed to fall below 1.30 MPa at any point throughout the thrust chamber wall. Figure 4.7 shows the typical pressure distributions of the three cases throughout the chamber wall. These results were obtained using an inlet mass flow rate of 0.095 kg/s and a hot gas boundary heat flux of 30,000 W/m². The results show that for the same mass flow rate, there is a larger pressure drop in the wall as the porosity

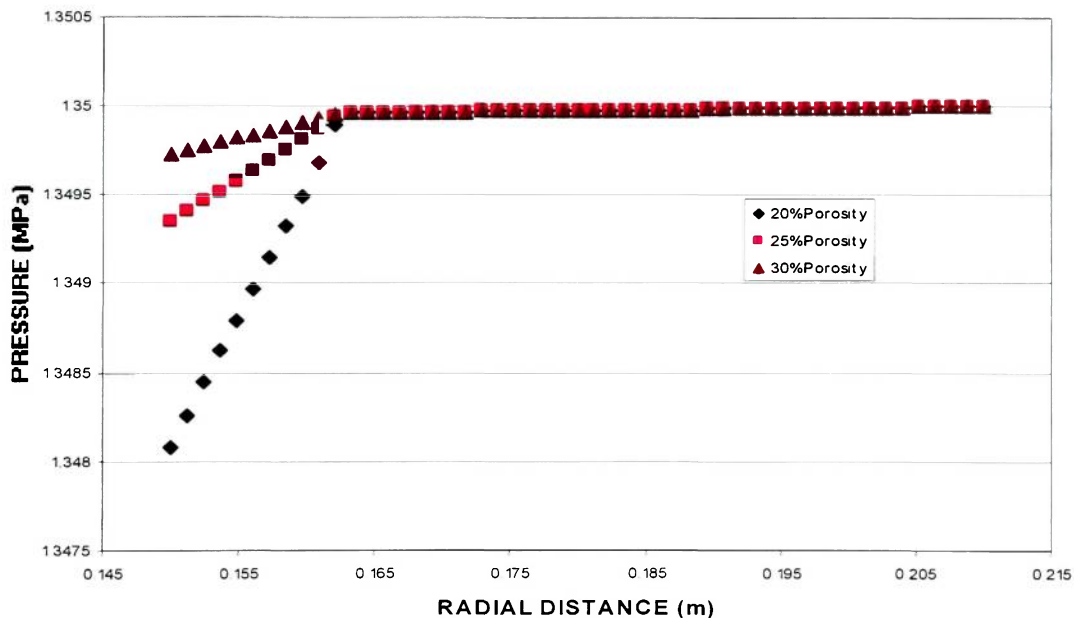


Figure 4.7: Pressure Distribution for the Varying Porosity Cases

Porosity	Maximum Mass Flow Rate (kg/s)
0.20	1.43
0.25	2.66
0.30	5.00

Table 4.4: Maximum Mass Flow Rates for Varying Liner Porosities

decreases. For any given inlet mass flow rate, a liner with a porosity of 0.30 provides the smallest pressure drop of the three cases that were tested. Table 4.4 shows the maximum inlet mass flow rates that can be used with a cold gas boundary of 1.35 MPa without requiring the pressure to drop below 1.30 MPa. As with the varying liner thickness cases, simulations were performed for the varying liner porosity cases with the same hot gas boundary heat flux and inlet mass flow rates. The hot gas boundary heat flux used was $30,000 \text{ W/m}^2$ and the inlet mass flow rates ranged from 0.095 kg/s to 1.14 kg/s. Figure 4.8 shows the pressure drop distributions for the three cases at the various inlet mass flow rates. The results for this analysis show similar behavior to the previous study where the

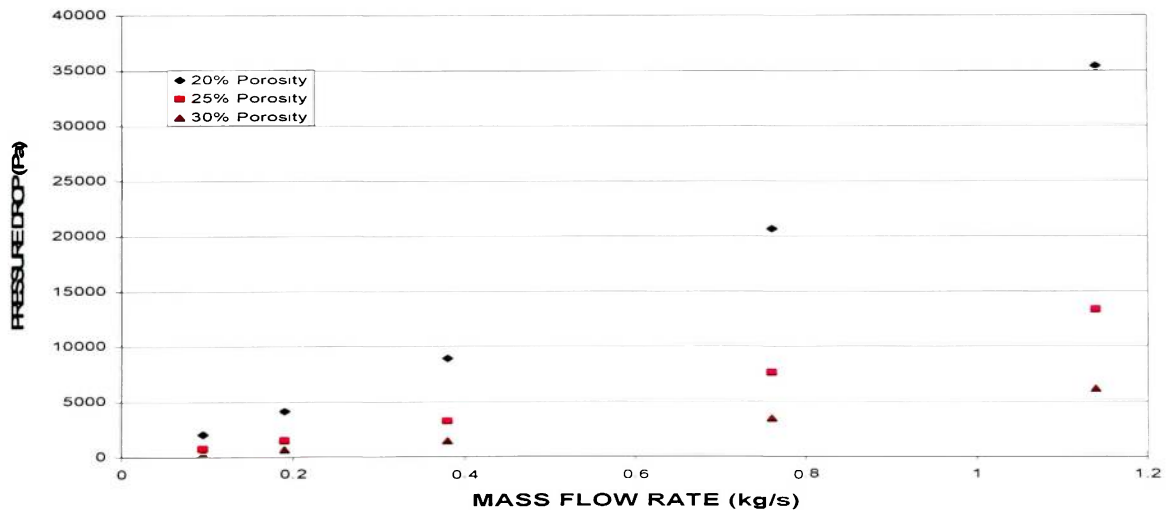


Figure 4.8: Pressure Drop Comparison for the Varying Liner Porosity Cases

liner thicknesses were varied. As the mass flow rate increases, the increase in the pressure drop is accelerated. There is a much more rapid increase in the pressure drop in the 20% porous liner than there is in the other two cases. The results show that a liner with a porosity of 0.30 has the smallest pressure drop and a liner with a porosity of 0.20 has the largest pressure drop for any given inlet mass flow rate. As mentioned in the previous section, when the porosity of the liner is altered, the permeability coefficients and effective thermal conductivity are altered. As the porosity increases, the permeability increases which decreases the resistance to flow of the fluid leading to a decrease in the pressure drop throughout the wall.

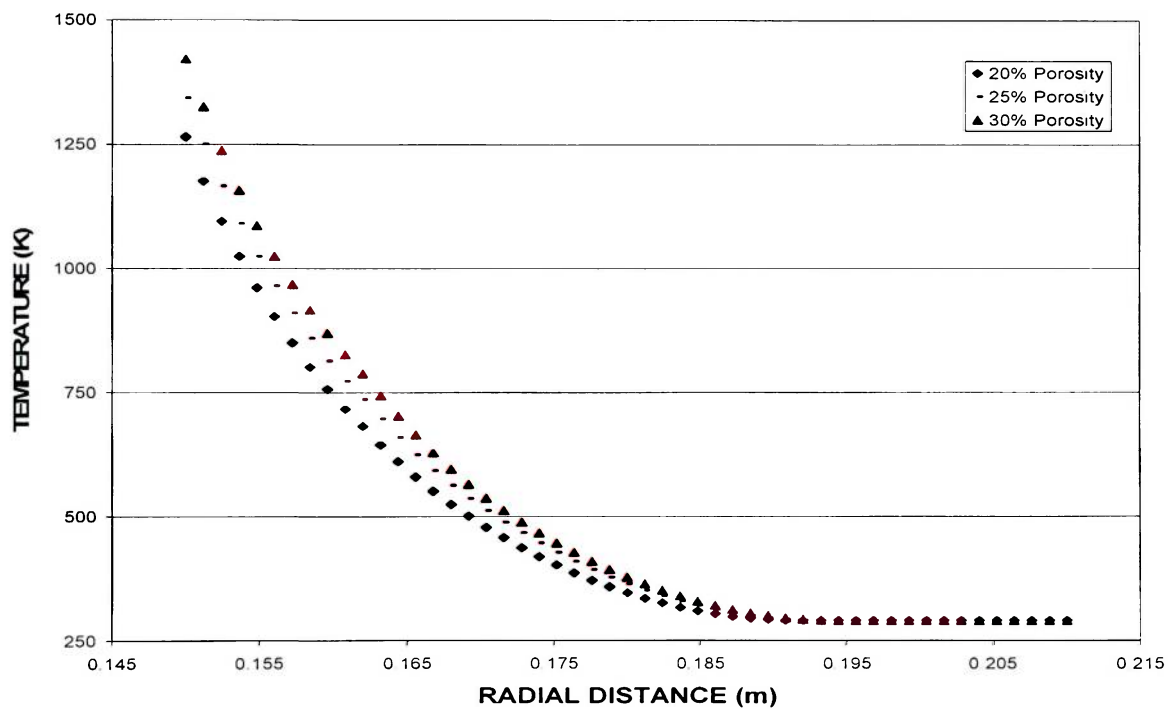


Figure 4.9: Typical Temperature Distribution for the Varying Liner Porosity Cases

The same tests that were performed in the previous study are now performed with the liner porosities being varied. Figure 4.9 shows the typical temperature distribution for the three cases. The inlet mass flow rate was set at 0.095 kg/s and the hot gas boundary

heat flux was set at $30,000 \text{ W/m}^2$. The results shown in Figure 4.9 remain consistent throughout the study. In every case studied, a liner with a porosity of 0.20 provides the lowest temperature distribution in the wall while a liner with a porosity of 0.30 provides the highest temperature distribution. More specifically, a liner with a lower porosity results in the smallest maximum temperature inside the wall for any given inlet mass flow rate with the same hot gas boundary heat flux. This is due to the difference in the effective thermal conductivity. As mentioned in the previous section, the effective thermal conductivity of the porous liner section and coolant increases as the porosity of the porous material decreases. In this study, the case where the liner has a porosity of 0.20 provides the largest effective thermal conductivity. Therefore it is able to conduct

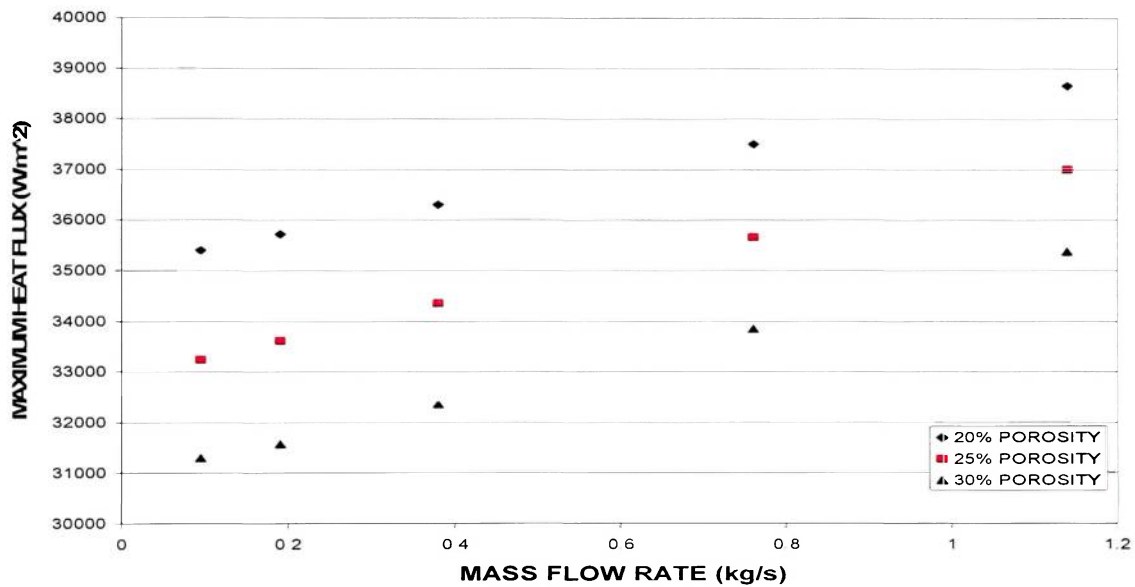


Figure 4.10: Maximum Heat Flux for the Different Liner Porosity Cases for Varying Porosity

heat away better from the hot gas boundary heat flux at various inlet mass flow rates for the different cases. For a given inlet mass flow rate a liner with a porosity of 0.20 will allow the maximum heat flux while a liner with a porosity of 0.30 will allow the smallest

maximum heat flux. The heat flux of the combustion products of a rocket engine can not be varied, but the magnitude of the heat flux will play a part on the parameters of the porous matrices. It was shown in Table 4.4 that a liner with a porosity of 0.30 can achieve the greatest inlet mass flow rates while maintaining a pressure drop of 50 kPa. The results of Table 4.5 show that it can also withstand the greatest hot gas boundary heat fluxes. The increased mass flow rate provides more supercritical hydrogen to the wall, which increases the magnitude of the advection term in the energy equation. Although a liner with a porosity of 0.20 provides the best temperature distribution throughout the wall among the porosity ranges studied, it can not be used under all circumstances. Ultimately, the thickness and porosity of the liner section will be determined by the overall design and performance requirements of the rocket.

Porosity	Maximum Heat Flux (W/m ²)
0.20	38950
0.25	42040
0.30	45855

Table 4.5: Maximum Allowable Heat Flux for the Various Liner Porosity Cases

Chapter 5: Conclusions and Recommendations

5.1 Conclusions

In this thesis the mathematical models and computer codes were developed for simulating the flow of a coolant and the transport phenomena in a transpiration cooled thrust chamber wall of a liquid rocket engine. This was done in two ways: by treating the coolant as an incompressible fluid and a compressible fluid in local thermal equilibrium with the porous structures that make up the thrust chamber wall. Finite difference method was used for solving the governing equations and predicting the steady-state behavior of the coolant fluid and the temperature distribution inside the thrust chamber wall. As expected, the simulations showed that as the mass flow rate of the coolant increases inside the wall, the overall temperature distribution decreases, allowing for a larger heat flux at the hot gas boundary. An increase in the mass flow rate also requires a larger pressure differential across the entire thickness of the thrust chamber wall and increases the overall magnitude of the Darcy velocity of the coolant inside the wall.

The incompressible flow model was run as a single porous layered system and given the same boundary conditions as the compressible flow model in an effort to determine if the incompressible flow model could be used to accurately predict the behavior of the fluid and the temperature of the system. With pressures of 1.35 MPa at the cold gas boundary and 1.31 MPa at the hot gas boundary, the mass flow rate of the incompressible model differed from the compressible flow model by a relative margin of 1.6% and the maximum difference in the system temperature at any node between the two models was a relative margin of 0.5%. The results of these simulations showed that the

incompressible flow model can be a very useful tool for determining the effects of transpiration cooling. The fact that the incompressible model produces results at a much faster rate than the compressible flow model makes the incompressible model a more practical and cheaper tool for future studies of transpiration cooling inside the thrust chamber wall of a liquid rocket engine.

Using the incompressible model, parametric studies were performed on a thrust chamber wall consisting of two layered porous matrices. The second layer that was used in the parametric studies was a porous liner also made of Si-C that is used to control the flow of the fluid inside the wall. The two main parametric analyses performed investigated the effects of varying the thickness and porosity of the porous liner section on the coolant behavior and temperature distribution inside the chamber wall.

The first case study involved varying the thickness of the porous liner section. The liner was modeled having a thickness that represented 10%, 20% and 30% of the total thrust chamber wall thickness. The results from these cases were also compared to results obtained when no porous liner was used. While the porous liner is primarily intended to provide structural support for the thrust chamber wall, the results show that there are cases where the use of the porous liner will provide a more efficient cooling technique than a thrust chamber wall consisting only of a single porous matrix. The results also show for a given mass flow rate that the pressure differential across the chamber wall increases as the thickness of the porous liner increases. This is a result of the porous liner section having a lower porosity, therefore having a lower permeability, than the porous

foam section which causes a larger pressure differential in the porous liner section. Naturally, as the thickness of the liner increases, the overall pressure differential in that region would increase.

The second case study involved varying the porosity of the porous liner section. The system was modeled with a porous liner having a porosity of 0.20, 0.25, and 0.30. As the porosity of the liner is increased, the permeability also increases causing a decrease in the resistance to the flow of the fluid. This resulted in a smaller pressure drop across the thrust chamber wall. The pressure difference applied across the thickness of the wall determines how large the inlet mass flow rate and ultimately the mass flow rate inside the thrust chamber wall will be. As the pressure differential increases, the mass flow rate increases. As more coolant is introduced into the thrust chamber wall, the temperature distribution is lowered due the increased volumetric heat capacity and effective thermal conductivity that comes with a larger amount of coolant. The results of this case show that the liner with a porosity of 0.20 provides the most efficient cooling option of the three cases that were studied. These results are consistent over the entire range of inlet mass flow rates for all three liner porosities investigated for conditions in which the coolant remained in supercritical state. The drawback is that the case where the liner has a porosity of 0.20 (lowest porosity considered) also requires a larger pressure differential than the other cases (higher porosities considered) for a specified inlet mass flow rate. As the porosity of the liner increases, the range of inlet mass flow rates that are possible also increases.

5.2 Recommendations

The incompressible flow model was used to perform the parametric studies due to large computer run-times that occurred when running the compressible flow model. With the use of more powerful computational resources, such as a Beowulf Cluster or CRAY supercomputers, the compressible flow model could be adapted to perform the parametric studies. This would also involve applying the more complex boundary conditions at the interface between the two porous layers. The models that were developed in this research assumed local thermal equilibrium between the porous matrix and coolant fluid. It is recommended that this constraint is relaxed and two energy equations for the fluid phase and the porous matrices are used to determine if that would have any significant effect. The parametric studies that were performed in this research used the same material for both the porous foam and porous liner. It is recommended that the parametric studies be enhanced to include different materials for either or both of the porous matrices as more materials are developed for different liquid rocket engine applications.

References

- Brockmeyer, J.W., Fortini, A.J., Williams, B.E., Tuffias, R.H. *High-Efficiency Open-Cell Foam Heat Exchangers for Actively Cooled Propulsion Components*, AIAA 1998-3441, 1998.
- Chi, S.W. *Heat Pipe Theory and Practice: A Sourcebook*. New York: McGraw-Hill Book Company, 1976.
- Greuel, D., Herbertz, A., Haidn, O.J., Ortelt, M., Hald, H. *Transpiration Cooling Applied to C/C Liners of Cryogenic Liquid Rocket Engines*, AIAA 2004-3682, July 11-14 2004, 40th AIAA/ASME/SAE/ASEE/JPC Conference and Exhibit.
- Landis, J.A. *Numerical Study of a Transpiration Cooled Rocket Nozzle*, Ph.D. thesis, Air Force Institute of Technology, December 1995, AFIT/GA/ENY/95D-01.
- Lezuo, M., Haidn O.J., *Transpiration Cooling Using Gaseous Hydrogen*, AIAA 1997-2209, 1997.
- Ngo, C.C., Lai, F.C. *Effective Permeability of a Layered Porous Annulus*, AIAA 1998-2676, 1998.
- Serbest, E., Haidn, O., Hald, H., Korger, G., Winkelmann, P. *Effusion Cooling in Rocket Combustors Applying Fiber Reinforced Ceramics*, AIAA 1999-2911, June 20-24 1999, 35th AIAA/ASME/SAE/ASEE/JPC Conference and Exhibit.
- Sozen, M. *Enhanced Heat Transfer and Pressure Drop Simulation in Round Tubes with Porous Inserts*, Technical Report, BEC-XFD/APS, Argonne National Laboratory, July 1994.
- Sutton, G., Biblarz, O. *Rocket Propulsion Elements, Seventh Edition*, Canada: John Wiley and Sons, 2001.
- Steel, S., Anderl, T. *Transpiration Cooling: Researchers develop transpiration-cooling concepts to improve rocket engine thrust chambers*, Technical Article, ML-03-12, Air Force Research Laboratory, 2004.

Appendix A: Discretization of the Governing Equations and Boundary Condition by Finite Difference Approximations for the Incompressible Flow Model

A.1 Continuity Equation for the Node NTOT-1

The simplified continuity equation is discretized at the point NTOT using backward differencing and then solved for the Darcy velocity of the fluid at point NTOT-1. The same process is used to determine the velocity at the node NINT-1.

$$\frac{\partial}{\partial r}(ru) = 0$$

$$\frac{3r_{NIOI}u_{NTOI} - 4r_{NTOT-1}u_{NIOI-1} + r_{NIOI-2}u_{NTOI-2}}{2\Delta r} = 0$$

$$u_{NTOI-1} = \frac{3r_{NTOT}u_{NIOI} + r_{NIOI-2}u_{NIOI-2}}{4r_{NIOI}}$$

A.2 Momentum Equation for the Node NTOT-1

The simplified momentum equation is discretized at the point NTOT using backward differencing in the pressure gradient term and then solved for the fluid pressure at the node NTOT-1. The same process is used to determine the pressure at the node NINT-1.

$$\frac{\partial P}{\partial r} = -\frac{\mu_f \varepsilon}{\alpha} u - \frac{\varepsilon^2 \rho}{\beta} |u|u$$

$$\frac{3P_{NTOI} - 4P_{NTOT-1} + P_{NTOT-2}}{2\Delta r} = -\frac{\mu_f \varepsilon}{\alpha} u_{NIOI} - \frac{\varepsilon^2 \rho}{\beta} |u_{NIOI}|u_{NIOI}$$

$$P_{NTOT-1} = \frac{(3P_{NIOI} + P_{NIOI-2})}{4} + \left(\frac{\Delta r \mu_f}{2\alpha}\right) u_{NIOI} + \left(\frac{\Delta r \rho_f}{2\beta}\right) |u_{NIOI}|u_{NIOI}$$

A.3 Continuity Equation for the Interior Nodes

This is the derivation for the Darcy velocity at a typical interior node starting with the simplified continuity equation and using upwind differencing.

$$\frac{\partial}{\partial r}(ru) = 0$$
$$\frac{-3r_n u_n + 4r_{n+1} u_{n+1} - r_{n+2} u_{n+2}}{2\Delta r} = 0$$
$$u_n = \frac{4r_{n+1} u_{n+1} - r_{n+2} u_{n+2}}{3r_n}$$

A.4 Momentum Equation for the Interior Nodes

This is the derivation for the fluid pressure at a typical interior node starting with the simplified momentum equation

$$\frac{\partial P}{\partial r} = -\frac{\mu_f \varepsilon}{\alpha} u - \frac{\varepsilon^2 \rho}{\beta} |u| u$$
$$\frac{-3P_n + 4P_{n+1} - P_{n+2}}{2\Delta r} = -\frac{\mu_f \varepsilon}{\alpha} u_n - \frac{\varepsilon^2 \rho}{\beta} |u_n| u_n$$
$$P_n = \frac{4P_{n+1} - P_{n+2}}{3} - \frac{2\Delta r \mu_f \varepsilon}{3\alpha} u_n - \frac{2\Delta r \varepsilon^2 \rho}{3\beta} |u_n| u_n$$

A.5 Velocity at the Interface Boundary

At the interface boundary between the two porous media, the velocity is determined through a mass balance across the boundary. Since the density is constant, there must be continuity in the Darcy velocity across the boundary.

$$u_1 = u_2$$

$$\frac{-3r_n u_n + 4r_{n+1} u_{n+1} - r_{n+2} u_{n+2}}{2\Delta r} = \frac{3r_n u_n - 4r_{n-1} u_{n-1} + r_{n-2} u_{n-2}}{2\Delta r}$$

$$6r_n u_n = -r_{n-2} u_{n-2} + 4r_{n-1} u_{n-1} + 4r_{n+1} u_{n+1} - r_{n+2} u_{n+2}$$

$$u_n = \frac{-r_{n-2} u_{n-2} + 4r_{n-1} u_{n-1} + 4r_{n+1} u_{n+1} - r_{n+2} u_{n+2}}{6r_n}$$

A.6 Pressure at the Interface Boundary

The momentum equation is used to implement the interface boundary condition that the fluid pressure must be continuous across the interface boundary.

$$P_1 = P_2$$

$$\frac{-3P_n + 4P_{n+1} - P_{n+2}}{2\Delta r} + \frac{\mu \varepsilon_1}{\alpha_1} u_n + \frac{\varepsilon_1^2 \rho}{\beta_1} |u_n| u_n = \frac{3P_n - 4P_{n-1} + P_{n-2}}{2\Delta r} + \frac{\mu \varepsilon_2}{\alpha_2} u_n + \frac{\varepsilon_2^2 \rho}{\beta_2} |u_n| u_n$$

$$\frac{6P_n + P_{n-2} - 4P_{n-1} - 4P_{n+1} + P_{n+2}}{2\Delta r} = \mu \left(\frac{\varepsilon_1}{\alpha_1} - \frac{\varepsilon_2}{\alpha_2} \right) u_n + \rho \left(\frac{\varepsilon_1^2}{\beta_1} - \frac{\varepsilon_2^2}{\beta_2} \right) |u_n| u_n$$

$$P_n = \left(\frac{-P_{n-2} + 4P_{n-1} + 4P_{n+1} - P_{n+2}}{6} \right) + \frac{\Delta r \mu}{3} \left(\frac{\varepsilon_1}{\alpha_1} - \frac{\varepsilon_2}{\alpha_2} \right) u_n + \frac{\Delta r \rho}{3} \left(\frac{\varepsilon_1^2}{\beta_1} - \frac{\varepsilon_2^2}{\beta_2} \right) |u_n| u_n$$

A.7 Energy Equation for Interior Nodes

The following is the derivation of the system temperature at a typical interior node. These expressions are valid for both the incompressible flow model and the compressible flow model. The derivation begins with the energy equation.

$$\left(\rho c_p \right)_A \frac{\partial T}{\partial t} + \varepsilon_A \rho_f u_f c_{p_f} \frac{\partial T}{\partial r} = \frac{1}{r} \frac{\partial}{\partial r} \left(k_A r \frac{\partial T}{\partial r} \right)$$

$$(\rho c_p)_A \left[\frac{T_n^{m+1} - T_n^m}{\Delta t} \right] = \frac{1}{r_n} \left[\frac{\left(r k_A \frac{\partial T}{\partial r} \right)_{n+1/2} - \left(r k_A \frac{\partial T}{\partial r} \right)_{n-1/2}}{\Delta r} \right] - \varepsilon_A \rho_n^m u_n^m c_{p_f} \left(\frac{T_{n+1}^m - T_{n-1}^m}{2\Delta r} \right)$$

$$(\rho c_p)_A \left[\frac{T_n^{m+1} - T_n^m}{\Delta t} \right] = \frac{1}{r_p} \left[\frac{r_{n+1/2} k_A \left(\frac{T_{n+1}^m - T_n^m}{\Delta r} \right) - r_{n-1/2} k_A \left(\frac{T_n^m - T_{n-1}^m}{\Delta r} \right)}{\Delta r} \right] - \varepsilon_A \rho_n^m u_n^m c_{p_f} \left(\frac{T_{n+1}^m - T_{n-1}^m}{2\Delta r} \right)$$

$$\frac{(\rho c_p)_A}{\Delta t} (T_n^{m+1} - T_n^m) = \left(\frac{\varepsilon_A \rho_n^m u_n^m c_{p_f}}{2\Delta r} - \frac{k_A r_{n-1/2}}{r_n \Delta r^2} \right) T_{n-1}^m + \left[\frac{k_A (r_{n+1/2} + r_{n-1/2})}{r_n \Delta r^2} \right] T_n^m$$

$$+ \left(\frac{k_A r_{n+1/2}}{r_n \Delta r^2} - \frac{\varepsilon_A \rho_n^m u_n^m c_{p_f}}{2\Delta r} \right) T_{n+1}^m$$

$$\frac{(\rho c_p)_A}{\Delta t} (T_n^{m+1} - T_n^m) = \frac{k_A}{r_n (\Delta r)^2} \left[r_{n+1/2} T_{n+1}^m + (r_{n+1/2} + r_{n-1/2}) T_n^m - r_{n-1/2} T_{n-1}^m \right]$$

$$- \varepsilon_A \rho_n^m u_n^m c_{p_f} \left(\frac{T_{n+1}^m - T_{n-1}^m}{2\Delta r} \right)$$

$$T_n^{m+1} = \left[\frac{\Delta t r_{n-1/2} k_A}{(\rho c_p)_A r_n \Delta r^2} + \frac{\Delta t \varepsilon_A \rho_n^m u_n^m c_{p_f}}{2(\rho c_p)_A \Delta r} \right] T_{n-1}^m + \left[1 - \frac{\Delta t \cdot (r_{n+1/2} + r_{n-1/2}) \cdot k_A}{(\rho c_p)_A \cdot r_n \cdot \Delta r^2} \right] \cdot T_n^m$$

$$+ \left[\frac{\Delta t r_{n+1/2} k_A}{(\rho c_p)_A r_n \Delta r^2} - \frac{\Delta t \varepsilon_A \rho_n^m u_n^m c_{p_f}}{2(\rho c_p)_A \Delta r} \right] T_{n+1}^m$$

A.8 Energy Balance at the Interface Boundary

This derivation solves for the temperature of the system at the interface boundary using an energy balance across the boundary.

$$k_1 \frac{\partial T_1}{\partial r} \Big|_{\text{Interface}} = k_2 \frac{\partial T_2}{\partial r} \Big|_{\text{Interface}}$$

$$k_1 \left(\frac{-3T_n^m + 4T_{n+1}^m - T_{n+2}^m}{2\Delta r} \right) = k_2 \left(\frac{3T_n^m - 4T_{n-1}^m + T_{n-2}^m}{2\Delta r} \right)$$

$$3k_2 T_n^m + 3k_1 T_n^m = k_2 T_{n-2}^m - 4k_2 T_{n-1}^m - 4k_1 T_{n+1}^m + k_1 T_{n+2}^m$$

$$T_n^{m+1} = \frac{1}{3 \cdot (k_1 + k_2)} \cdot \left[-k_2 \cdot T_{n-2}^{m+1} + 4 \cdot k_2 \cdot T_{n-1}^{m+1} + 4 \cdot k_1 \cdot T_{n+1}^{m+1} - k_1 \cdot T_{n+2}^{m+1} \right]$$

A.9 Energy Balance at the Hot Gas Boundary

This derivation determines the temperature of the system at the hot gas boundary using an energy balance at the boundary. A heat flux is specified at the hot gas boundary. These expressions are valid for both the incompressible and compressible flow models.

$$q'' = k_2 \left. \frac{\partial T}{\partial r} \right|_{HGB}$$

$$q'' = k_2 \left(\frac{3T_n^{m+1} - 4T_{n+1}^{m+1} + T_{n+2}^{m+1}}{2\Delta r} \right)$$

$$T_n^{m+1} = -\frac{1}{3} T_{n+2}^{m+1} + \frac{4}{3} T_{n+1}^{m+1} - \left(\frac{2\Delta r}{3k_2} \right) q''$$

Appendix B: Discretization of the Governing Equations and Boundary Condition by Finite Difference Approximations for the Compressible Flow Model

B.1 Continuity Equation for the Interior Nodes

The unsteady continuity equation is used to solve for the fluid density at any typical interior node in the wall in the compressible flow model.

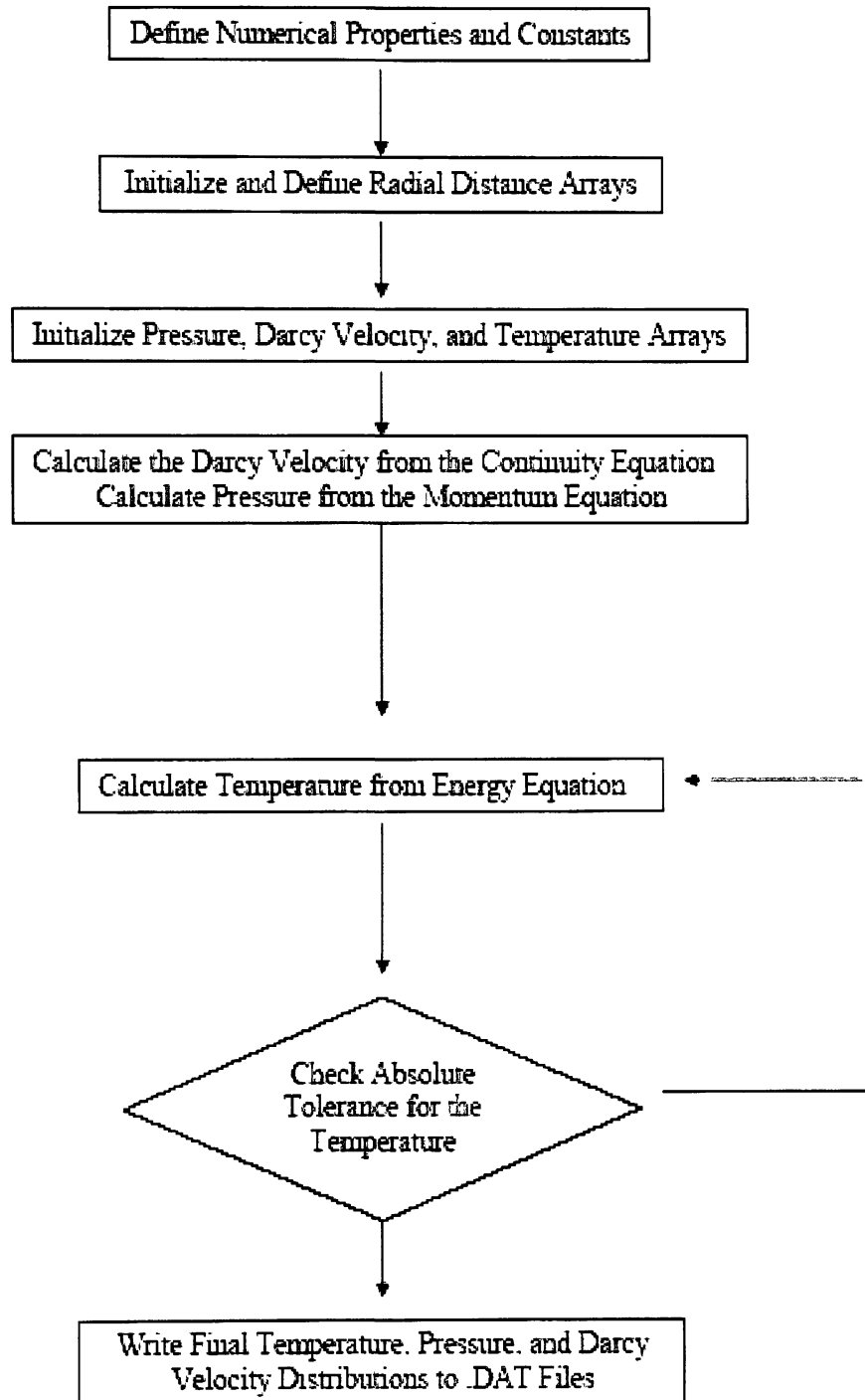
$$\begin{aligned} \varepsilon \frac{\partial \rho_f}{\partial t} + \frac{1}{r} \frac{\partial}{\partial r} (r \rho_f u_f) &= 0 \\ \varepsilon \left(\frac{\rho_n^{m+1} - \rho_n^m}{\Delta t} \right) &= -\frac{1}{r_n} \left(\frac{r_{n+1} \rho_{n+1}^m u_{n+1}^m - r_n \rho_n^m u_n^m}{\Delta r} \right) \\ \rho_n^{m+1} &= \rho_n^m - \frac{\Delta t}{\varepsilon r_n} \left(\frac{r_{n+1} \rho_{n+1}^m u_{n+1}^m - r_n \rho_n^m u_n^m}{\Delta r} \right) \\ \rho_n^{m+1} &= \left[1 + \frac{\Delta t u_n^m}{\varepsilon \Delta r} \right] \rho_n^m - \left[\frac{\Delta t r_{n+1} u_{n+1}^m}{\varepsilon_A r_n \Delta r} \right] \rho_{n+1}^m \end{aligned}$$

B.2 Momentum Equation for the Interior Nodes

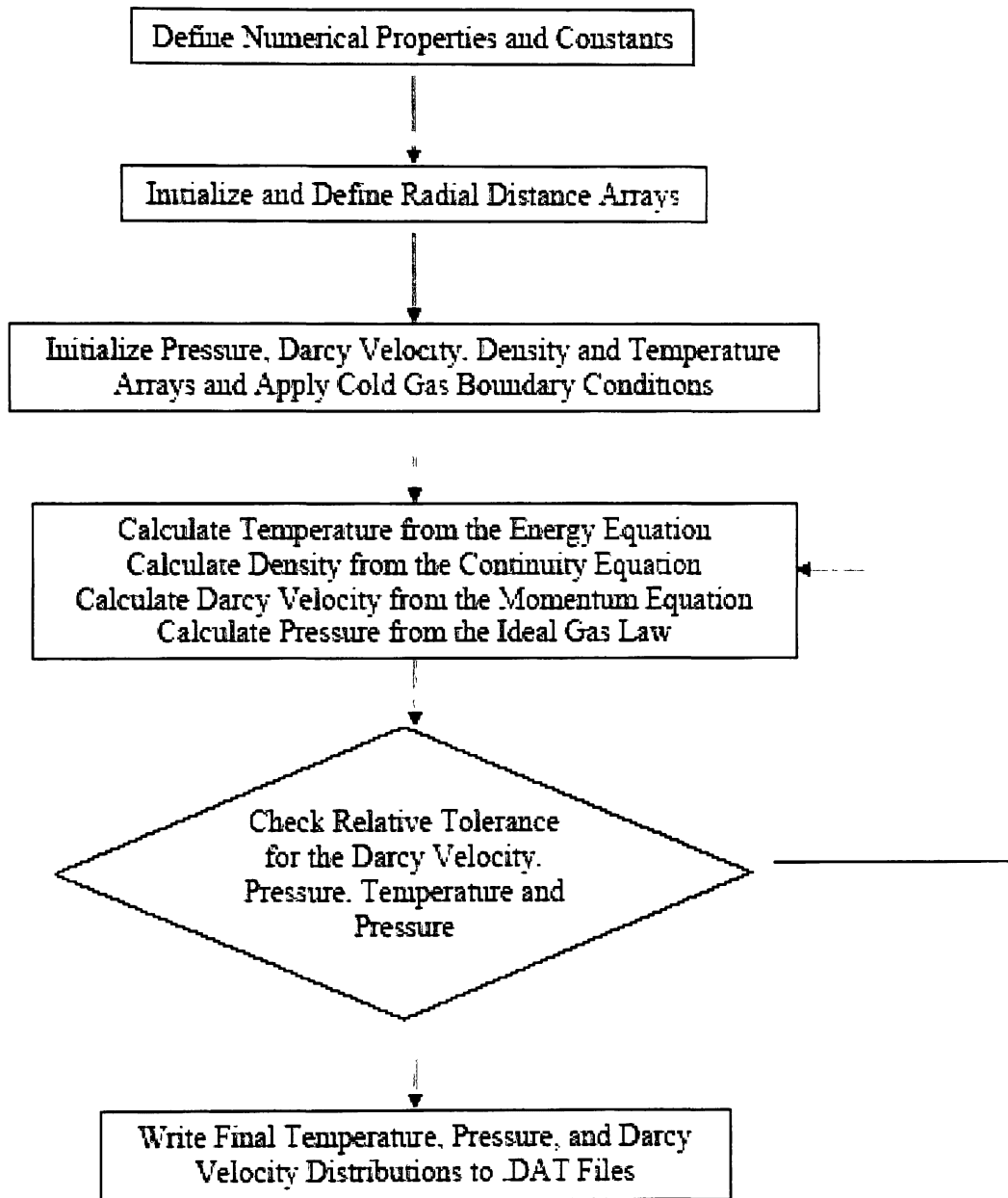
The unsteady momentum equation is used to solve for the Darcy velocity at any typical interior node in the wall in the compressible flow model.

$$\begin{aligned} \frac{1}{\varepsilon_A} \frac{\partial}{\partial t} (\rho_f u_f) &= -\frac{\partial P_f}{\partial r} - \left(\frac{\mu_f}{\alpha_A} + \frac{\rho_f}{\beta_A} |u_f| \right) \cdot u_f \\ \frac{\rho_n^{m+1} u_n^{m+1} - \rho_n^m u_n^m}{\Delta t} &= -\varepsilon \left(\frac{P_n^m - P_{n-1}^m}{\Delta r} \right) - \frac{\varepsilon \mu}{\alpha} u_n^m - \frac{\varepsilon \rho_n^m}{\beta} |u_n^m| u_n^m \\ \rho_n^{m+1} u_n^{m+1} &= \rho_n^m u_n^m - \frac{\Delta t \varepsilon}{\Delta r} (P_n^m - P_{n-1}^m) - \frac{\Delta t \varepsilon \mu}{\alpha} u_n^m - \frac{\Delta t \varepsilon \rho_n^m}{\beta} |u_n^m| u_n^m \\ u_n^{m+1} &= \frac{1}{\rho_n^{m+1}} \left[\left(1 - \frac{\varepsilon \Delta t}{\beta} |u_n^m| \right) \rho_n^m u_n^m - \frac{\varepsilon \cdot \Delta t \mu_f}{\alpha} u_n^m - \frac{\varepsilon \Delta t}{\Delta r} (P_n^m - P_{n-1}^m) \right] \end{aligned}$$

Appendix C: Incompressible Flow Model FORTRAN Flowchart



Appendix D: Compressible Flow Model FORTRAN Flowchart



Appendix E: Incompressible Flow Model FORTRAN Program

```
PROGRAM INCOMP
C
C THIS PROGRAM WILL ANALYZE THE FLUID BEHAVIOR THROUGHOUT
C THE WALL ASSUMING AN INCOMPRESSIBLE FLUID
C
C FIRST I AM GOING TO DECLARE THE CONSTANTS THAT WILL BE
C USED THROUGHOUT THE PROGRAM. THESE VALUES WILL GENERALLY
C BE MATERIAL PROPERTIES. ALL VALUES WILL BE DOUBLE
C PRECISION.
C
C KF IS THE THERMAL CONDUCTIVITY OF THE COOLANT
C KS1 IS THE THERMAL CONDUCTIVITY OF THE POROUS FOAM
C KS2 IS THE THERMAL CONDUCTIVITY OF THE POROUS LINER
C EPS1 IS THE POROSITY OF THE POROUS FOAM
C EPS2 IS THE POROSITY OF THE POROUS LINER
C DPORE1 IS THE MEAN PORE DIAMETER OF THE POROUS FOAM
C DPORE2 IS THE MEAN PORE DIAMETER OF THE POROUS LINER
C ALPHA AND BETA ARE PERMEABILITY CONSTANTS
C MUF IS THE VISCOSITY OF THE COOLANT
C CPF IS THE SPECIFIC HEAT CAPACITY OF THE COOLANT
C C1 IS THE HEAT CAPACITY OF THE POROUS FOAM
C C2 IS THE HEAT CAPACITY OF THE POROUS LINER
C RHOS IS THE DENSITY OF THE POROUS MATRIX
C RF IS THE GAS CONSTANT USED IN STATE EQUATION
C K1 IS THE EFFECTIVE THERMAL CONDUCTIVITY IN THE FOAM
C K2 IS THE EFFECTIVE THERMAL CONDUCTIVITY IN THE LINER
C QHOT IS THE HEAT FLUX ON THE HOT GAS SIDE BOUNDARY
C RHOF IS THE DENSITY OF THE COOLANT FLUID
C
      DOUBLE PRECISION KF,KS1,KS2,EPS1,EPS2,ALPHA1,ALPHA2
      DOUBLE PRECISION DPORE1,DPORE2,BETA1,BETA2,MUF,CPF
      DOUBLE PRECISION CS1,CS2,RHOS1,RHOS2,RF,SIZE,QHOT
      DOUBLE PRECISION DR,R,RPLUS,RMINUS,TOLD,TNEW,DP
      DOUBLE PRECISION DT,RHOF,PCOLD,P.U, POLD,UOLD,
      DOUBLE PRECISION TIME,K1,K2,C1,C2,TDIFF
      DOUBLE PRECISION MAXEPS,EPS,R0,RTOT,MDOT,ATOT,PI
      DOUBLE PRECISION MAXDU,MAXDP,UEPS,PEPS,UDIFF,PDIFF
      REAL TSTART,TEND,PROC
C
C R IS THE RADIUS ARRAY
C RPLUS IS THE R+1/2 ARRAY
C RMINUS IS THE R-1/2 ARRAY
C
      DIMENSION R(51)
```

```

        DIMENSION RPLUS(51)
        DIMENSION RMINUS(51)
C
C TNEW AND TOLD ARE THE TEMPERATURE ARRAYS
C PNEW AND POLD ARE THE PRESSURE ARRAYS
C UNEW AND UOLD ARE THE VELOCITY ARRAYS
C RHONEW AND RHOOLD ARE THE DENSITY ARRAYS
C
        DIMENSION TNEW(51),TOLD(51)
        DIMENSION P(51),U(51)
        DIMENSION POLD(51),UOLD(51)
C
C TDIFF IS THE DIFFERENCE BETWEEN THE OLD AND NEW
C TEMPERATURES AT EACH NODE
C DIFSQ IS THE SQUARE OF THE TEMPERATURE DIFFERENCE AT EACH
C NODE
C
        DIMENSION TDIFF(51),PDIFF(51),UDIFF(51)
C
        CALL CPU_TIME(TSTART)
C
        PI=3.1416
        KF=.200
        KS1=1.0
        KS2=1.0
        EPS1=.50
        EPS2=.50
        DPORE1=.000635
        DPORE2=.000635
        MUF=8.6E-6
        RF=4125
        CPF=14.7
        C1=1422.6
        C2=1422.6
        RHOS1=3200.00
        RHOS2=3200.00
        QHOT=30200.00
C
        ALPHA1=(DPORE1**2*EPS1**3)/(150*(1-EPS1)**2)
        ALPHA2=(DPORE2**2*EPS2**3)/(150*(1-EPS2)**2)
        BETA1=(DPORE1*EPS1**3)/(1.75*(1-EPS1))
        BETA2=(DPORE2*EPS2**3)/(1.75*(1-EPS2))
C
        K1=(KF*((2.0*KF+KS1)-2.0*(1-EPS1)*(KF-KS1))/(2.0*KF+KS1+
        +((1-EPS1)*(KF-KS1))))
C

```

```

      K2=(KF*((2.0*KF+KS2)-2.0*(1-EPS2)*(KF-KS2))/(2.0*KF+KS2+
      +((1-EPS2)*(KF-KS2))))
C
C
C INITIALIZING THE ARRAYS
C
C R0 IS THE RADIUS OF THE THRUST CHAMBER
C
      R0=0.15
C
C SIZE IS THE TOTAL LENGTH OF THE WALL IN METERS
C
      SIZE=.06
C
C RTOT IS THE TOTAL RADIUS
C
      RTOT=R0+SIZE
C
C NTOT REFERS TO THE TOTAL NUMBER OF POINTS
C
      NTOT=51
C
C DR IS THE CHANGE IN RADIUS
C
      DR=SIZE/(NTOT-1)
C
C NINT REFERS TO THE POINT WHICH REPRESENTS THE INTERIOR
C BOUNDARY
C
      NINT=11
C
C PCOLD IS THE COLD GAS BOUNDARY PRESSURE
C
      PCOLD=1350E3
C
C MDOT IS THE MASS FLOW RATE AT THE COLD GAS BOUNDARY WHICH
C WILL DETERMINE THE VELOCITY AT THE COLD GAS BOUNDARY
C
      MDOT=0.3775
C
C ATOT IS THE TOTAL SURFACE AREA OF THE ENGINE
C
      ATOT=PI*RTOT*2.0
C
C RHOF IS THE FLUID DENSITY
C

```

```

        RHOF=1.20
C
C R IS THE RADIUS ARRAY
C
        R(1)=R0
        DO 10 N=2,NTOT
        R(N)=R(N-1)+DR
    10 CONTINUE
C
C RPLUS IS THE R+1/2 RADIUS ARRAY
C
        DO 20 N=2,(NTOT),1
        RPLUS(1)=R0
        RPLUS(N)=R(N)+(DR/2.0)
    20 CONTINUE
C
C RMINUS IS THE R-1/2 RADIUS ARRAY
C
        DO 30 N=2,(NTOT),1
        RMINUS(1)=R0
        RMINUS(N)=R(N)-(DR/2.0)
    30 CONTINUE
C
C INPUTING INITIAL GUESS
C
C TOLD IS THE INITIAL TEMPERATURE GUESS
C
        DO 40 N=1,NTOT
        TOLD(N)=290.00
    40 CONTINUE
C
C FIRST I AM GOING TO LOOP TO CALCULATHE THE VELOCITY AND
C PRESSURE AND RUN THE LOOPS UNTIL A TOLERANCE IS MET NOTE
C THAT THESE VALUES ARE INDEPENDANT OF TEMPERATURE SO THEY
C ARE CALCULATED BY THEMSELVES
C
C NOW THE VALUES AT THE COLD GAS BOUNDARY WILL BE
C CALCULATED. THESE VALUES ARE ALWAYS CONSTANT
C
    45 N=NTOT
        P(N)=PCOLD
        U(N)=-MDOT/( RHOF*ATOT)
C
C NOW I WILL CALCULATE THE VALUES AT THE NODE JUST BEFORE THE
C COLD GAS BOUNDARY
C

```

```

N=NTOT-1
U(N)=(3*R(N+1)*U(N+1)+R(N-1)*U(N-1))/(4*R(N))
P(N)=PCOLDA(N,DR,MUF,ALPHA1,BETA1,RHOF,U,P)
C
C THE NEXT LOOP CALCULATES THE NEW PROPERTIES INSIDE THE
C POROUS FOAM USING THE FOAM FUNCTIONS
C
DO 50 N=1,NTOT-2
U(N)=(4*R(N+1)*U(N+1)-R(N+2)*U(N+2))/(3*R(N))
P(N)=PFOAM(N,DR,MUF,ALPHA1,BETA1,RHOF,U,P)
C
50 CONTINUE
C
C THE NEXT LOOP CALCULATES THE DIFFERENCE BETWEEN THE OLD
C VALUES AND THE NEW VALUES
C UDIFF IS THE DIFFERENCE BETWEEN THE OLD AND NEW VELOCITY
C PDIFF IS THE DIFFERENCE BETWEEN THE NOE AND OLD PRESSURE
C UEPS IS THE CURRENT MAXIMUM UDIFF
C PEPS IS THE CURRENT MAXIMUM PDIFF
C MAXDU IS THE MAXIMUM ALLOWABLE UDIFF
C MAXDP IS THE MAXIMUM ALLOWABLE PDIFF
C
PEPS=0.0
UEPS=0.0
MAXDP=1E-7
MAXDU=1E-7
M=M+1
C
DO 70 N=1,NTOT
C
PDIFF(N)=P(N)-POLD(N)
IF (PDIFF(N).GT.PEPS) PEPS=PDIFF(N)
C
UDIFF(N)=U(N)-UOLD(N)
IF (UDIFF(N).GT.UEPS) UEPS=UDIFF(N)
70 CONTINUE
C
C THE NEXT IF STATEMENT WILL TEST IF THE TOLERANCE IS MET
C
IF (PEPS-MAXDP) 75,75,80
75 IF (UEPS-MAXDU) 90,90,80
C
80 DO 85 N=1,NTOT

```

```

C
      UOLD(N)=U(N)
      POLD(N)=P(N)
C
      85 CONTINUE
      GOTO 45
C
      90 CONTINUE
C
C NOW THE VELOCITY AND PRESSURE DISTRIBUTIONS ARE COMPLETED.
C SINCE NEITHER OF THESE PROPERTIES ARE BASED ON TEMPERATURE
C OR TIME. THIS METHOD OF CALCULATION IS ALLOWED. NEXT COME
C THE TEMPERATURE LOOPS
C
C DT IS THE CHANGE IN TIME
C TIME IS THE TOTAL TIME TAKEN
C
      DT=1E-4
      TIME=0.0
C
C FIRST WILL COME THE TEMPERATURE AT THE HOT GAS BOUNDARY
C WHICH IS CONSTANT THROUGHOUT
C
      95 TNEW(NTOT)=TOLD(NTOT)
C
C NEXT THE TEMPERATURE IN THE POROUS FOAM
C
      DO 100 N=2,NTOT-1
      TNEW(N)=TFOAM(N,DT,DR,R,RMINUS,RPLUS,EPS1,CPF,RHOF,U,C1,K1,
&RHOS1,TOLD)
      100 CONTINUE
C
C NOW THE TEMPERATURE IN THE POROUS LINER
C
      DO 110 N=2,NINT-1
      TNEW(N)=TLINER(N,DT,DR,R,RMINUS,RPLUS,EPS2,CPF,RHOF,
&U,C2,K2,RHOS2,C1,TOLD)
      110 CONTINUE
C
C NOW THE TEMPERATURE AT THE INTERIOR BOUNDARY
C
      N=NINT
      TNEW(N)=TINT(N,K1,K2,TNEW)
C
C NEXT THE HOT GAS BOUNDARY TEMPERATURE
C

```



```

      N=1
      TNEW(N)=THOT(N,TNEW,DR,K2,QHOT)
C
      TIME=TIME+DT
C
C NOW I WILL CALCULATE THE DIFFERENCES FOR THE TOLERANCE
C TDIFF IS THE DIFFERENCE BETWEEN THE NEW AND OLD
C TEMPERATURES
C EPS IS THE CURRENT MAXIMUM TDIFF
C MAXEPS IS THE MAXIMUM ALLOWABLE TDIFF, OR THE TOLERANCE
C LEVEL
C
      EPS=0.0
      MAXEPS=1E-7
      M=M+1
C
      DO 120 N=1,NTOT
      TDIFF(N)=TNEW(N)-TOLD(N)
      IF (TDIFF(N).GT.EPS) EPS=TDIFF(N)
120 CONTINUE
C
C
C THE NEXT IF STATEMENT WILL TEST IF THE TOLERANCE IS MET
C
      IF (EPS-MAXEPS) 140,140,130
C
130 DO 135 N=1,NTOT
C
      TOLD(N)=TNEW(N)
C
135 CONTINUE
      GOTO 95
C
140 CONTINUE
C
C
      WRITE(*,*) TIME
C
      OPEN(6,FILE='VELOCITY.DAT')
      OPEN(7,FILE='TEMP.DAT')
      OPEN(8,FILE='PRESSURE.DAT')
C
      DO 150 N=1,NTOT
      WRITE(6,*) U(N)
      WRITE(7,*) TNEW(N)
      WRITE(8,*) P(N)

```

```

150 CONTINUE
C
    CALL CPU_TIME(TEND)
    PROC=TEND-TSTART
    WRITE(*,*) PROC
    END
C
C THAT IS THE END OF THE MAIN PROGRAM
C NEXT ARE THE FUNCTIONS THAT ARE CALLED
C
C PCOLDA CALCULATES THE PRESSURE AT THE NODE JUST BEFORE THE
C COLD GAS BOUNDARY
C
    FUNCTION PCOLDA(N,DR,MUF,ALPHA1,BETA1,RHOF,U,P)
C
    DOUBLE PRECISION DR,MUF,ALPHA1,BETA1,RHOF,U,P,A,B,C
    DIMENSION P(51),U(51)
C
    A=DR*MUF/ALPHA1
    B=DR*RHOF/BETA1
    C=(3*P(N+1)+P(N-1))/4
C
    PCOLDA=C+A*U(N+1)+B*U(N+1)*ABS(U(N+1))
C
    RETURN
    END
C
C PFOAM CALCULATES THE PRESSURE INSIDE THE POROUS FOAM
C
    FUNCTION PFOAM(N,DR,MUF,ALPHA1,BETA1,RHOF,U,P)
C
    DOUBLE PRECISION DR,MUF,ALPHA1,BETA1,RHOF,U,P,A,B,C
    DIMENSION P(51),U(51)
C
    A=DR*MUF/ALPHA1
    B=DR*RHOF/BETA1
    C=(4*P(N+1)-P(N+2))/3
C
    PFOAM=C+A*U(N)+B*U(N)*ABS(U(N))
C
    RETURN
    END
C
C PFOAMA CALCULATES THE PRESSURE AT THE NODE NINT-1
C
    FUNCTION PFOAMA(N,DR,MUF,ALPHA2,BETA2,RHOF,U,P)

```

```

C
DOUBLE PRECISION DR,MUF,ALPHA2,BETA2,RHOF,U,P,A,B,C
DIMENSION P(51),U(51)
C
A=DR*MUF/ALPHA2
B=DR*RHOF/BETA2
C=(3*P(N+1)+P(N-1))/4
C
PFOAMA=C+A*U(N+1)+B*U(N+1)*ABS(U(N+1))
C
RETURN
END
C
C PLINER CALCULATES THE PRESSURE INSIDE THE POROUS LINER
C
FUNCTION PLINER(N,DR,MUF,ALPHA2,BETA2,RHOF,U,P)
C
DOUBLE PRECISION DR,MUF,ALPHA2,BETA2,RHOF,U,P,A,B,C
DIMENSION P(51),U(51)
C
A=DR*MUF/ALPHA2
B=DR*RHOF/BETA2
C=(4*P(N+1)-P(N+2))/3
C
PLINER=C+A*U(N)+B*U(N)*ABS(U(N))
C
RETURN
END
C
C UINT CALCULATES THE VELOCITY AT THE INTERIOR BOUNDARY
C
FUNCTION UINT(N,R,U)
C
DOUBLE PRECISION R,U,A,B,C
DIMENSION R(51),U(51)
C
A=4*R(N+1)*U(N+1)+4*R(N-1)*U(N-1)
B=-R(N-2)*U(N-2)-R(N+2)*U(N+2)
C=6*R(N)
C
UINT=(A+B)/C
C
RETURN
END
C
C PINT CALCULATES THE PRESSURE AT THE INTERIOR BOUNDARY

```

```

C
    FUNCTION PINT(N,DR,MUF,BETA1,BETA2,ALPHA1,ALPHA2,P,U,
&RHOF)
C
    DOUBLE PRECISION DR,MUF,BETA1,BETA2
    DOUBLE PRECISION ALPHA1,ALPHA2,P,U,RHOF,A,B,C
    DIMENSION P(51),U(51)
C
    A=(-P(N+2)+4*P(N+1)+4*P(N-1)-P(N-2))/6
    B=(DR*MUF/3)*(1/ALPHA1-1/ALPHA2)
    C=(DR*RHOF/3)*(1/BETA1-1/BETA2)
C
    PINT=A+B*U(N)+C*U(N)*ABS(U(N))
C
    RETURN
    END
c
C THIS FUNCTION CALCULATES THE TEMPERATURE AT THE INTERIOR
POROUS
C FOAM NODES.
C
    FUNCTION TFOAM(N,DT,DR,R,RMINUS,RPLUS,EPS1,CPF,RHOF,U,C1,
& K1,RHOS1,TOLD)
C
    DOUBLE PRECISION DT,DR,R,RMINUS,RPLUS,EPS1,CPF,RHOF,U,C1,K1
    DOUBLE PRECISION RHOS1,TOLD,A,B,C,RHOC
    DIMENSION R(51),RMINUS(51),RPLUS(51)
    DIMENSION U(51),TOLD(51)
C
    RHOC=(RHOS1*C1*(1-EPS1))+(EPS1*RHOF*CPF)
C
    A=((DT*RMINUS(N)*K1)/(RHOC*R(N)*DR*DR))+((DT*EPS1*RHOF*
+U(N)*CPF)/(2.0*RHOC*DR))
C
    B=1-(DT*((RMINUS(N)+RPLUS(N))*K1)/(RHOC*R(N)*DR*DR))
C
    C=((DT*RPLUS(N)*K1)/(RHOC*R(N)*DR*DR))-((DT*EPS1*RHOF*
+U(N)*CPF)/(2.0*RHOC*DR))
C
    TFOAM=(A*TOLD(N-1))+(B*TOLD(N))+(C*TOLD(N+1))
C
    RETURN
    END
C
C THIS FUNCTION CALCULATES THE TEMPERATURE IN THE LINER
C

```

```

FUNCTION TLINER(N,DT,DR,R,RMINUS,RPLUS,EPS2,CPF,
& RHOF,U,C2,K2,RHOS2,C1,TOLD)
C
DOUBLE PRECISION DT,DR,R,RMINUS,RPLUS,EPS2,CPF,RHOF,U,C2,K2
DOUBLE PRECISION RHOS2,C1,TOLD,A,B,C,RHOC
DIMENSION R(51),RMINUS(51),RPLUS(51)
DIMENSION U(51),TOLD(51)
C
RHOC=(RHOS2*C2*(1-EPS2))+(EPS2*RHOF*CPF)
C
A=((DT*RMINUS(N)*K2)/(RHOC*R(N)*DR*DR))+((DT*EPS2*RHOF*
+U(N)*CPF)/(2.0*RHOC*DR))
C
B=1-(DT*((RMINUS(N)+RPLUS(N))*K2)/(RHOC*R(N)*DR*DR))
C
C=((DT*RPLUS(N)*K2)/(RHOC*R(N)*DR*DR))-((DT*EPS2*RHOF*
+U(N)*CPF)/(2.0*RHOC*DR))
C
TLINER=(A*TOLD(N-1))+(B*TOLD(N))+(C*TOLD(N+1))
C
RETURN
END
C
C THIS FUNCTION CALCULATES THE TEMPERATURE AT THE BOUNDARY
C BETWEEN THE 2 POROUS MATRICEWS
C
FUNCTION TINT(N,K1,K2,TNEW)
C
DOUBLE PRECISION K1,K2,TNEW
DIMENSION TNEW(51)
C
TINT=(1/(3*(K1+K2)))*(-K1*TNEW(N-2)+4*K1*TNEW(N-
+1)+4*K2*TNEW(N+1)-K2*TNEW(N+2))
C
RETURN
END
C
C THIS FUNCTION CALCULATES THE TEMPERATURE AT THE HOT GAS SIDE
BOUNDARY
C
FUNCTION THOT(N,TNEW,DR,K2,QHOT)
DOUBLE PRECISION TNEW,DR,K2,QHOT
DIMENSION TNEW(51)
C
THOT=-((TNEW(N+2)/3)+(4*TNEW(N+1)/3)+(2*DR*QHOT/(3*K2))

```

RETURN
END

Appendix F: Compressible Flow Model FORTRAN Program

```
PROGRAM COMP
C
C
C THIS IS THE PROGRAM THAT DETERMINES THE FLOW OF THE FLUID
C USING THE
C COMPRESSIBLE FLOW MODEL
C
C FIRST I AM GOING TO DECLARE THE CONSTANTS THAT WILL BE
C USED THROUGHOUT THE PROGRAM. THESE VALUES WILL GENERALLY
C BE MATERIAL PROPERTIES. ALL VALUES WILL BE DOUBLE
C PRECISION.
C
C KF IS THE THERMAL CONDUCTIVITY OF THE COOLANT
C KS1 IS THE THERMAL CONDUCTIVITY OF THE POROUS FOAM
C EPS1 IS THE POROSITY OF THE POROUS FOAM
C DPORE1 IS THE MEAN PORE DIAMETER OF THE POROUS FOAM
C ALPHA AND BETA ARE PERMEABILITY CONSTANTS
C MUF IS THE VISCOSITY OF THE COOLANT
C CPF IS THE SPECIFIC HEAT CAPACITY OF THE COOLANT
C C1 IS THE HEAT CAPACITY OF THE POROUS FOAM
C RHOS IS THE DENSITY OF THE POROUS MATRIX
C RF IS THE GAS CONSTANT USED IN STATE EQUATION
C K1 IS THE EFFECTIVE THERMAL CONDUCTIVITY IN THE FOAM
C QHOT IS THE HEAT FLUX ON THE HOT GAS SIDE BOUNDARY
C
C DOUBLE PRECISION KF,KS1,EPS1,ALPHA1
C DOUBLE PRECISION DPORE1,BETA1,MUF,CPF
C DOUBLE PRECISION CS1,RHOS1,RF,SIZE,QHOT
C DOUBLE PRECISION DR,R,RPLUS,RMINUS,TOLD,TNEW,POLD
C DOUBLE PRECISION PNEW,UOLD,UNEW,RHOOLD,RHONNEW,DT
C DOUBLE PRECISION TIME,K1,C1,TDIFF,PEPS,UEPS,RHOEPS
C DOUBLE PRECISION MAXDP,MAXDU,MAXRHO,PDIFF,UDIFF,RHODIF
C DOUBLE PRECISION MAXEPS,EPS,R0,NPLUS,NMINUS,B
C REAL TSTART,TEND,PROC
C
C R IS THE RADIUS ARRAY
C RPLUS IS THE R+1/2 ARRAY
C RMINUS IS THE R-1/2 ARRAY
C
C DIMENSION R(51)
C DIMENSION RPLUS(51)
C DIMENSION RMINUS(51)
C
C TNEW AND TOLD ARE THE TEMPERATURE ARRAYS
```

```

C PNEW AND POLD ARE THE PRESSURE ARRAYS
C UNEW AND UOLD ARE THE VELOCITY ARRAYS
C RHONEW AND RHOOLD ARE THE DENSITY ARRAYS
C
    DIMENSION TNEW(51),TOLD(51)
    DIMENSION PNEW(51),POLD(51)
    DIMENSION UOLD(51),UNEW(51)
    DIMENSION RHOOLD(51),RHONEW(51)
C
C TDIFF IS THE DIFFERENCE BETWEEN THE OLD AND NEW
C TEMPERATURES AT EACH NODE
C DIFSQ IS THE SQUARE OF THE TEMPERATURE DIFFERENCE AT EACH
C NODE
C
    DIMENSION TDIFF(51)
C
    CALL CPU_TIME(TSTART)
C
    KF=0.1683
    KS1=1.00
    EPS1=.50
    DPORE1=.000635
    MUF=.0000086
    RF=4124
    CPF=29.00/2.00
    C1=1422.6
    RHOS1=3200.00
    QHOT=30000.00
    M=1
C
    ALPHA1=(DPORE1**2*EPS1**3)/(150*(1-EPS1)**2)
C
    BETA1=(DPORE1*EPS1**3)/(1.75*(1-EPS1))
C
    K1=KF*(2*KF+KS1-2*((1-EPS1)*(KF-KS1)))/(2*KF+KS1+(1-EPS1)*
    +(KF-KS1))
C
C INITIALIZING THE ARRAYS
C
C R0 IS THE RADIUS OF THE THRUST CHAMBER
C
    R0=0.15
C
C SIZE IS THE TOTAL LENGTH OF THE WALL IN METERS
C

```



```

        SIZE=.06
C
C NTOT REFERS TO THE TOTAL NUMBER OF POINTS
C
        NTOT=51
C
C DR IS THE CHANGE IN RADIUS
C
        DR=SIZE/(NTOT-1)
C
C R IS THE RADIUS ARRAY
C
        R(1)=R0
        DO 10 N=2,NTOT
        R(N)=R(N-1)+DR
10 CONTINUE
C
C RPLUS IS THE R+1/2 RADIUS ARRAY
C
        DO 20 N=1,(NTOT),1
        RPLUS(N)=R(N)+(DR/2.0)
20 CONTINUE
C
C RMINUS IS THE R-1/2 RADIUS ARRAY
C
        DO 30 N=1,(NTOT),1
        RMINUS(N)=R(N)-(DR/2.0)
30 CONTINUE
C
C INPUTING INITIAL GUESS
C
C TOLD, POLD, UOLD, AND RHOOLD NEED INITIAL VALUES IN ORDER
C TO CALCULATE NEW VALUES AND RUN THE ANALYSIS.
C
C INITIAL TEMPERATURE DISTRIBUTION GUESS
C
        DO 40 N=1,NTOT
        TOLD(N)=290.00
40 CONTINUE
C
C INITIAL PRESSURE GUESS
C
        DO 50 N=1,NTOT
        POLD(N)=1300E3
50 CONTINUE
C

```

```

C INITIAL DENSITY GUESS
C
      DO 60 N=1,NTOT
      RHOOLD(N)=POLD(N)/(RF*TOLD(N))
60 CONTINUE
C
C INITIAL VELOCITY GUESS
C
      DO 70 N=1,NTOT
      UOLD(N)=0.0
70 CONTINUE
C
C NOW TO RUN THE LOOPS TO CALCULATE THE NEW PROPERTIES
C
C DT IS THE CHANGE IN TIME
C TIME IS THE TOTAL TIME TAKEN
C
      DT=1E-7
      TIME=0.0
C
C NEXT I WILL CALL THE DIFFERENT FUNCTIONS CORRESPONDING TO
C WHICH PART OF THE WALL I AM ANALYZING
C
C THE COLD GAS SIDE BOUNDARY CONDITIONS ARE FIRST
C
75  N=NTOT
C
      TNEW(NTOT)=TOLD(NTOT)
      PNEW(N)=1350E3
      RHONEW(N)=PNEW(N)/(RF*TOLD(N))
      UNEW(N)=UCOLD(N,POLD,DT,DR,UOLD,RHONEW,ALPHA1,BETA1,
&RHOOLD,EPS1,MUF)
C
C THE NEXT LOOP CALCULATES THE NEW PROPERTIES INSIDE THE
C POROUS FOAM USING THE FOAM FUNCTIONS
C
      DO 80 N=2,NTOT-1
C
      TNEW(N)=TFOAM(N,DT,DR,R,RMINUS,RPLUS,EPS1,CPF,RHOOLD,UOLD
&RHOS1,TOLD,C1,K1,)
C
      RHONEW(N)=RHOFOA(N,DT,R,UOLD,EPS1,DR,RHOOLD)
      UNEW(N)=UFOAM(N,DT,EPS1,RHONEW,DR,POLD,RHOOLD,ALPHA1,
&MUF,BETA1,UOLD)
C
      PNEW(N)=RHONEW(N)*RF*TNEW(N)

```

```

C
  80 CONTINUE
C
C NEXT IS THE HOT GAS BOUNDARY PROPERTIES
C THE PRESSURE AT THIS BOUNDARY IS HELD CONSTANT THROUGHOUT
C THE ENTIRE ANALYSIS
C
  N=1
C
  TNEW(N)=THOT(N,TNEW,DR,K1,QHOT)
  PNEW(N)=1310E3
  RHONEW(N)=PNEW(N)/(RF*TNEW(N))
  UNEW(N)=UHOT(N,POLD,DT,DR,UOLD,RHONEW,ALPHA1,BETA1,EPS1,
&RHOOLD,MUF)
C
C
C THE NEXT LOOP CALCULATES THE DIFFERENCE BETWEEN THE OLD
C AND THE NEW PROPERTY VALUES AND DETERMINE THE MAXIMUM
C DIFFERENCES FOR EACH OF THE PROPERTIES. THE PROPERTIES ARE
C INITIALLY SET TO 0.0
C
  EPS=0.0
  PEPS=0.0
  UEPS=0.0
  RHOEPS=0.0
C
  DO 90 N=1,NTOT
C
  TDIFF(N)=ABS((TNEW(N)-TOLD(N))/TOLD(N))
  IF(TDIFF(N).GT.EPS) EPS=TDIFF(N)
C
  PDIFF(N)=ABS((PNEW(N)-POLD(N))/POLD(N))
  IF(PDIFF(N).GT.PEPS) PEPS=PDIFF(N)
C
  UDIFF(N)=ABS((UNEW(N)-UOLD(N))/UOLD(N))
  IF(UDIFF(N).GT.UEPS) UEPS=UDIFF(N)
C
  RHODIF(N)=ABS((RHONEW(N)-RHOOLD(N))/RHOOLD(N))
  IF(RHODIF(N).GT.RHOEPS) RHOEPS=RHODIF(N)
  90 CONTINUE
C
C MAXEPS IS THE MAXIMUM VALUE FOR THE DIFFERENCE, OR THE MAX
C TOLERANCE
C
  MAXEPS=1E-4
  MAXDP=1E-4

```

```

MAXDU=1E-4
MAXRHO=1E-4
C
C NEXT I WILL CHECK EACH VALUE TO SEE IF THEIR TOLERANCE IS MET
C
    IF(EPS-MAXEPS) 100,100,130
    100 IF(PEPS-MAXDP) 110,110,130
    110 IF(UEPS-MAXDU) 120,120,130
    120 IF(RHOEPS-MAXRHO) 180,180,130
    130 CONTINUE
C
C
C THE NEXT IF STATEMENT IS A CREATED COUNTER. AFTER EACH 1
C MILLION TIME STEPS,THERE WILL BE A COUNTER PRINTED ON THE
C SCREEN STARTING AT 1 AND INCREASING BY 1FOR EACH MILLION TIME
C STEPS THAT ARE PERFORMED THIS STEP WAS ADDED SO I CAN
C VISUALLY SEE THAT THE COMPILER IS STILL RUNNING AND HAS NOT
C STALLED
C
    IF (A*1E6-M) 140,140,150
    140 WRITE (*,*) M/(1E6)
        A=A+1
    150 CONTINUE
C
C THE NEXT DO LOOP WILL TAKE THE NEW PARAMETERS AND WILL SET
C THEM AS OLD VALUES FOR THE NEW CALCULATIONS
C
    160 DO 170 N=1,NTOT
        TOLD(N)=TNEW(N)
        POLD(N)=PNEW(N)
        RHOOLD(N)=RHONEW(N)
        UOLD(N)=UNEW(N)
    170 CONTINUE
C
    GOTO 75
C
    180 CONTINUE
C
C
C NEXT I AM CREATING TEXT FILES TO WRITE THE PROPERTIES TO
C
    OPEN(6,FILE='VELOCITY.DAT')
    OPEN(7,FILE='TEMP.DAT')
    OPEN(8,FILE='DENSITY.DAT')
    OPEN(9,FILE='PRESSURE.DAT')
C

```

```

C THE NEXT DO LOOP WRITES THE PROPERTIES IN THEIR RESPECTIVE
C FILES AND IS SET UP
C TO WRITE THE VALUE FOR EACH RESPECTIVE NODE ON ITS OWN LINE
C IN THE TEXT FILE IN ORDER STARTING FROM NODE 1 CORRESPONDING
C TO THE HOT GAS BOUNDARY
C
      DO 190 N=1,NTOT
C
      WRITE(6,*) UNEW(N)
      WRITE(7,*) TNEW(N)
      WRITE(8,*) RHONEW(N)
      WRITE(9,*) PNEW(N)
C
190 CONTINUE
C
C
C FINALLY I FINISH THE RUN TIME FUNCTION AND PRINT THE TOTAL CPU
C RUN TIME TO THE SCREEN AS WELL AS THE SIMULATION TIME
C
      CALL CPU_TIME(TEND)
      PROC=TEND-TSTART
      WRITE(*,*) PROC
      WRITE(*,*) TIME
      END
C
C THAT IS THE END OF THE MAIN PROGRAM. BELOW ARE THE FUNCTIONS
C THAT ARE CALLED THROUGHOUT THE PROGRAM IN THE LOOPS
C
C THIS FUNCTION CALCULATES THE TEMPERATURE IN THE INTERIOR
C NODES
C
      FUNCTION TFOAM(N,DT,DR,R,RMINUS,RPLUS,EPS1,CPF,RHOOLD,
&UOLD,C1,K1RHOS1,TOLD)
C
      DOUBLE PRECISION DT,RPLUS,EPS1,CPF,RHOOLD,UOLD,C1,K1
      DOUBLE PRECISION RHOS1,TOLD,A,B,C,RHOC,DR,R,RMINUS
      DIMENSION R(51),RMINUS(51),RPLUS(51)
      DIMENSION RHOOLD(51),UOLD (51),TOLD(51)
C
      RHOC=(RHOS1*C1*(1-EPS1))+(EPS1*RHOOLD(N)*CPF)
C
      A=((DT*RMINUS(N)*K1)/(RHOC*R(N)*DR*DR))+((DT*EPS1*
+RHOOLD(N)*UOLD(N)*CPF)/(2.0*RHOC*DR))
C
      B=1-(DT*((RMINUS(N)+RPLUS(N))*K1)/(RHOC*R(N)*DR*DR))
C

```

```

C      C=((DT*RPLUS(N)*K1)/(RHOC*R(N)*DR*DR))-((DT*EPS1*RHOOLD(N)*
+UOLD(N)*CPF)/(2.0*RHOC*DR))
C
C      TFOAM=(A*TOLD(N-1))+(B*TOLD(N))+(C*TOLD(N+1))
C
C      RETURN
C      END
C
C THIS FUNCTION CALCULATES THE FLUID DENSITY IN THE INTERIOR
C NODES
C
C      FUNCTION RHOFOA(N,DT,R,UOLD,EPS1,DR,RHOOLD)
C
C      DOUBLE PRECISION DT,R,UOLD,EPS1,DR,RHOOLD,A,B
C      DIMENSION R(51),UOLD(51),RHOOLD(51)
C
C      A=1+(DT*UOLD(N)/(EPS1*DR))
C
C      B=(R(N+1)*UOLD(N+1)*DT)/(EPS1*R(N)*DR)
C
C      RHOFOA=A*RHOOLD(N)-B*RHOOLD(N+1)
C
C      RETURN
C      END
C
C THIS FUNCTION CALCULATES THE DARCY VELOCITY IN THE INTERIOR
C NODES
C
C      FUNCTION UFOAM(N,DT,EPS1,RHONEW,DR,POLD,RHOOLD,
&ALPHA1,BETA1,UOLD,MUF)
C
C      DOUBLE PRECISION DT,EPS1,RHONEW,DR,POLD,RHOOLD
C      DOUBLE PRECISION MUF,A,B,C,ALPHA1,BETA1,UOLD
C      DIMENSION RHONEW(51),POLD(51)
C      DIMENSION UOLD(51),RHOOLD(51)
C
C      A=(1-EPS1*DT*ABS(UOLD(N)))/BETA1)*RHOOLD(N)*UOLD(N)
C      B=(EPS1*DT*MUF/ALPHA1)*UOLD(N)
C      C=(EPS1*DT/DR)*(POLD(N)-POLD(N-1))
C
C      UFOAM=(A-B-C)/(RHONEW(N))
C
C      RETURN
C      END
C
C NOW FOR THE FUNCTIONS AT THE BOUNDARIES

```

```

C
C THIS NEXT FUNCTION CALCULATES THE DARCY VELOCITY AT
C THE COLD GAS BOUNDARY VELOCITY
C
    FUNCTION UCOLD(N,POLD,DT,DR,UOLD,RHONNEW,ALPHA1,
    &BETA1,EPS1,MUF,RHOOLD)
C
    DOUBLE PRECISION MUF,DT,DR,UOLD,RHONNEW,ALPHA1
    DOUBLE PRECISION RHOOLD,A,B,C,BETA1,EPS1,POLD
    DIMENSION RHOOLD(51),POLD(51)
    DIMENSION RHONNEW(51),UOLD(51)
C
    A=(1-EPS1*DT*ABS(UOLD(N))/BETA1)*RHOOLD(N)*UOLD(N)
    B=(EPS1*DT*MUF/ALPHA1)*UOLD(N)
    C=(EPS1*DT/DR)*(POLD(N)-POLD(N-1))
C
    UCOLD=(A-B-C)/RHONNEW(N)
C
    RETURN
    END
C
C THIS FUNCTION CALCULATES THE TEMPERATURE AT THE HOT GAS SIDE
C BOUNDARY
C
    FUNCTION THOT(N,TNEW,DR,K1,QHOT)
C
    DOUBLE PRECISION TNEW,DR,K1,QHOT
    DIMENSION TNEW(51)
C
    THOT=-((TNEW(N+2)/3)+(4*TNEW(N+1)/3)+(2*DR*QHOT/(3*K1)))
C
    RETURN
    END
C
C THIS FUNCTION CALCULATES THE DARCY VELOCITY AT THE HOT GAS
C BOUNDARY
C
    FUNCTION UHOT(N,POLD,DT,DR,UOLD,RHONNEW,ALPHA1,
    &BETA1,EPS1,MUF,RHOOLD)
C
    DOUBLE PRECISION MUF,DT,DR,UOLD,RHONNEW,ALPHA1
    DOUBLE PRECISION RHOOLD,A,B,C,BETA1,EPS1,POLD
    DIMENSION RHOOLD(51),POLD(51)
    DIMENSION RHONNEW(51),UOLD(51)
C
    A=(1-EPS1*DT*ABS(UOLD(N))/BETA1)*RHOOLD(N)*UOLD(N)

```

```
      B=(EPS1*DT*MUF/ALPHA1)*UOLD(N)
      C=(EPS1*DT/DR)*(POLD(N+1)-POLD(N))
C
      UHOT=(A-B-C)/RHONEW(N)
C
      RETURN
      END
```